Politecnico di Torino

Politecnico di Torino

MSc in Physics of Complex Systems

Variational Monte Carlo study of a two-orbital Hubbard model for iron-based superconductors

Candidate: Gabriele Gatti

matr. 317770

Supervisor: Prof. Luca F. Tocchio

Academic Year 2023/24

Acknowledgement

I would like to thank Politecnico di Torino for the wonderful five years devoted to study here. A special thank goes to Prof. Luca F. Tocchio and Dr. Vito Marino for guidance, enlightening discussions, time and patience. Computational resources were provided by HPC@POLITO (http://www.hpc.polito.it).

Contents

Introduction

The discovery of iron-based superconductors (IBS) opened a new path to study high-temperature superconductivity. Like cuprates, IBS are layered systems made of FeAs layers, where the Fe atoms form a square lattice. The low-energy properties of IBS are determined by electrons in d shells, where the competition beetween kinetic energy and electron-electron correlations determines the behavior of the material. The presence of strong correlations makes the BCS theory of superconductivity inadequate to describe the behavior of such materials. Indeed, the critical temperature value predicted by BCS is much smaller than the one measured in experiments. This implies that high-temperature superconductivity is not of phononic origin; instead, it might come from spin fluctuations of the electrons. It has been observed that superconductivity emerges when the parent compound is taken out of half filling by *doping* it (i.e. charge carriers are injected in the system). Therefore, since parent compounds of many transition metal oxides are Mott insulators, there is a correlation between high-temperature superconductivity and Mott physics. In multi-band materials it has recently been highlighted the effect of Hund's coupling (J). Hund's coupling is the exchange interaction between electrons in the same atom; its effect is to lower the cost in Coulomb energy when placing the electrons in different orbitals with parallel spin. This shakes the idea of Mottness being the sole origin of strong correlations, and suggests that there is another class of strongly correlated materials, which have been named Hund's metals. For multi-orbital shells, such as those of IBS, Hund's coupling lowers the effect of fluctuations favoring states with the highest possible spin on each transition metal ion.

A simple model to describe electrons interacting with each other in a lattice is the Hubbard model. In the case of IBS we have to consider all five d orbitals of Iron, since the crystalline structure of IBS is an hybrid between a tetrahedral and a tetragonal one. However, calculations on the five-orbital model are impossible to this day, hence a simplified approach has been tried considering only three orbitals, from the splitting between orbitals in the crystalline structure. From calculations of the Fermi surface it emerged that it is determined mainly by only two of the orbitals considered d_{xz}, d_{yz}; hence the proposal of the two-orbital model that is addressed in this thesis.

The Hamiltonian of such model is given by:

$$\begin{aligned}\mathcal{H} &= \mathcal{H}_0 + \mathcal{H}_K \\ \mathcal{H}_0 &= \sum_{\mathbf{q},\alpha,\beta,\sigma} t_{\mathbf{q}}^{\alpha,\beta} c_{\mathbf{q},\alpha,\sigma}^{\dagger} c_{\mathbf{q},\beta,\sigma}.\end{aligned} \tag{1}$$

$\mathcal{H}_0$ is the non interacting part of the Hamiltonian. $t_{\mathbf{q}}^{\alpha,\beta}$ are the hoppings in Fourier space, $\mathbf{q}$ is a vector in Fourier space, α, β are orbital indices and σ is the spin index. $\mathcal{H}_K$ is the Kanamori Hamiltonian and contains the interactions of the model i.e. Coulomb interaction and Hund's coupling and reads:

$$\begin{aligned}\mathcal{H}_K = & U \sum_{i,\alpha} n_{i,\alpha,\uparrow} n_{i,\alpha,\downarrow} \\ & + (U - 2J) \sum_{i,\sigma\neq\sigma'} \sum_{\alpha<\beta} n_{i,\alpha,\sigma} n_{i,\beta,\sigma'} \\ & + (U - 3J) \sum_{i,\sigma} \sum_{\alpha<\beta} n_{i,\alpha,\sigma} n_{i,\beta,\sigma} \\ & - J \sum_{i,\sigma\neq\sigma'} \sum_{\alpha<\beta} c_{i,\alpha,\sigma}^{\dagger} c_{i,\alpha,\sigma'} c_{i,\beta,\sigma'}^{\dagger} c_{i,\beta,\sigma} \\ & - J \sum_{i} \sum_{\alpha<\beta} (c_{i,\alpha,\uparrow}^{\dagger} c_{i,\alpha,\downarrow}^{\dagger} c_{i,\beta,\uparrow} c_{i,\beta,\downarrow}^{\dagger} + H.c.).\end{aligned} \tag{2}$$

The aim of this work is to study the effect of electron-electron correlations and understanding how they influence the superconductive behavior of the model. Therefore, we resort to Jastrow-Slater variational wavefunctions to approximate the ground state of the model and to Monte Carlo methods to compute expectation values over the variational state. The state of our model will be:

$$|\Psi\rangle = \mathcal{J}_C \mathcal{J}_S |\Psi_0\rangle. \tag{3}$$

where $\mathcal{J}_C, \mathcal{J}_S$ are the Jastrow factors and $|\Psi_0\rangle$ is the uncorrelated state of the model. The uncorrelated state is the ground-state of Hamiltonian $\mathcal{H}_0$ with additional intra-orbital pairing to describe the possible emergence of superconductivity, namely:

$$\mathcal{H}_{BCS} = \mathcal{H}_0 - \sum_{R,\alpha,\sigma} \mu_\alpha c_{R,\alpha,\sigma}^{\dagger} c_{R,\alpha,\sigma} + \sum_{R,\alpha,\delta} [\Delta_{\alpha,\delta} (c_{R,\alpha,\uparrow} c_{R+\delta,\alpha,\downarrow} - c_{R,\alpha,\downarrow} c_{R+\delta,\alpha,\uparrow} + h.c.)], \tag{4}$$

where $\delta \in (x, y, x+y, x-y)$ indicates nearest and next-nearest neighbors. R indicates a site in the lattice, while μ_α is the chemical potential of orbital α. $\Delta_{\alpha,\delta}$ and μ_α are optimized along the VMC run while the hoppings in $\mathcal{H}_0$ are kept constant.

We then introduce the two Jastrow factors in order to take into account electron-electron correlations, i.e:

$$\begin{aligned}\mathcal{J}_C &= \exp\left[-\frac{1}{2} \sum_{i,j,\alpha,\beta} v_{i,j}^{\alpha,\beta} (n_{i,\alpha,\uparrow} + n_{i,\alpha,\downarrow})(n_{j,\beta,\uparrow} + n_{j,\beta,\downarrow})\right] \\ \mathcal{J}_S &= \exp\left[\sum_i u_i S_{i,xz}^z S_{i,yz}^z\right],\end{aligned} \tag{5}$$

where $n_{i,\alpha,\uparrow} + n_{i,\alpha,\downarrow}$ and $S_{i,\alpha}^z = (n_{i,\alpha,\uparrow} - n_{i,\alpha,\downarrow})/2$ are respectively the electron density and spin along the z axis on site i and orbital α. The parameters $v_{i,j}^{\alpha,\beta}$ and u_i are the pseudo-potentials to

be optimized along the VMC run. The factor $\mathcal{J}_C$ is the charge density factor and encodes in the model the long range correlations, which are fundamental for Mott physics. The factor $\mathcal{J}_S$ is the spin factor and includes Hund's coupling.

The starting point of our analysis is the study of the Fermi surface without correlations and we find out that it it is made of two electron-like pockets and two hole-like pockets, in agreement with what has been found in previous calculations for the two-orbital model. However there are some differences with respect to calculations taking into account a larger number of orbitals. For instance: in the five-orbital model the two hole pockets are centered around point $(0, 0)$, instead in the two-orbital model one is centered at $(0, 0)$ and the other around (π, π)

Moved by results previously obtained for the three-orbital model, we are interested in finding out not only the emergence of superconductivity, but also if there exists a link between superconductivity and orbital selectivity. The latter corresponds to a different occupation of the involved orbitals. We then study the wavefunction on a 6×6 lattice, with two orbitals per site, in different doping regimes: half-filling, 10% hole/electron-*doping* and 20% hole/electron-*doping*. Our results show that orbital selectivity appears in the 10% hole-*doping* regime for the d_{xz} orbital, while the two orbitals have the same occupation in the other doping regimes investigated. Orbital selectivity is also paired with non zero BCS variational parameters at high values of U, necessary requisite for superconductivity.

In order to compute superconductive correlations we need to move to a larger lattice, hence we consider a 12×12 lattice. We investigate again the different regimes mentioned above using as initial state both one with a broken symmetry between the two orbitals and a uniform one. In all regimes, we get uniform solutions for the orbital occupations, i.e. no orbital selectivity, and in most cases BCS variational parameters are oscillating around zero. We then investigate superconductive correlations studying the correlation between two pairs of electrons, made by nearest-neighbors electrons along y, while one moves along x and the other remains fixed in place. Results show that in almost all cases the correlations rapidly fall to zero, in agreement with the absence of optimal BCS variational parameters in the variational wavefunction; hence we can say that also in the two-orbital model holds the fact that there cannot be orbital selectivity without superconductivity.

With our results we can confirm that there is a deep link between orbital selectivity and superconductivity since the latter cannot exist without the former. This means that the two-orbital model is insufficient to have a correct description of the IBS since it does not allow for the emergence of superconductivity in any doping regime. We ascribe this behavior to the lack of the d_{xy} orbital in the model, that could be instead crucial to account for the effect of the Hund's coupling.

Chapter 1

Metals, insulators and superconductivity

1.1 Band theory

Band theory has been the first successful theoretical approach to describe metals and insulators. According to this theory, the atoms of a solid are arranged in a lattice; while nuclei and inner electrons are fixed in their site, the electrons belonging to the outer shell are free to move through the lattice. In this system, of course, electrons are subject to the Coulomb interaction resulting from the nuclei and all the other electrons, making the equations of the system unsolvable without some approximation.

In this sense, a mean-field approach has been tried, in which the Coulomb interaction has been replaced by an effective single-particle lattice periodic potential representing the average interaction felt by each electron due to the presence of all the others. Thanks to this approach each electron can be treated as an independent particle. Solving the Schrödinger equation under such assumption in a lattice gives a set of electronic states $E_n(\mathbf{q})$ named as bands. These states depend only on the momentum $\mathbf{q}$ and are labeled by the band index n; also each band can host electrons up to two times the number of sites of the lattice due to spin degeneracy. The ground state of such system is obtained by filling the bands, in ascending order of energy, with electrons. The filling of the highest occupied band determines the behavior of the material. If the highest occupied band is partially filled, meaning that there is some space for electrons to move, the material will be a metal, while, if the highest occupied band is completely filled, electrons will not be able to move and the material will be an insulator.

From this theory, it is also possible to derive a rule to determine whether a material can be an insulator or not; indeed, if the number of electrons in the unit cell is odd than the highest occupied band will at least have a vacancy, implying that the material is a metal. This means that every

material made of atoms with an odd number of electrons in their unit cell is predicted to be a metal; however experiments showed that some materials, such as transition-metal oxides, behave as insulators despite having an odd number of electrons per unit cell. The reason for this failure can be traced out to the approximation made in first place, indeed to explain what is happening in those anomalous materials we need to take into account the Coulomb interactions.
The study of such anomalous materials gave rise to the concept of strongly-correlated electron systems.

1.2 Metal-Mott insulator transition

The materials predicted to be metals by band theory, but that actually behave as insulators have been defined as Mott insulators (Mott (1949)). This anomalous behavior stems from the fact that in these materials the repulsion between electrons prevails over their kinetic energy, making more convenient for the electrons to localize on different sites; thus leading to an insulating behavior when all sites are occupied by one electron (i.e. when the band is half filled), and therefore making possible that a material with an odd number of electrons per unit cell behaves like an insulator.
As an example, let us consider an atom with one electron in the $1s$ orbital with energy ϵ. When a second electron is added, the total energy of the system will be $2\epsilon + U$, where U represents the Coulomb interaction between them, thus leading to two different energy levels: one at energy ϵ and one at $\epsilon + U$. If we extend this reasoning to a lattice, instead of a single atom, the result is that, due to the Coulomb repulsion, the electronic band splits in two bands named Hubbard bands. By increasing the strength of the Coulomb interaction a gap opens between these two bands leading to the Mott-insulator state.

1.3 BCS theory

The BCS theory, developed in 1957 by Bardeen, Cooper and Schriffer, is the microscopic theory that describes the phenomenon of superconductivity as the condensation of Cooper pairs.

1.3.1 Cooper pairs

Let us consider a filled fermi sphere $|\Psi_0\rangle$ as the ground state of a weekly interacting model, meaning that electrons occupy all the states up to the Fermi energy ϵ_F. In 1956 (Cooper (1956)) Cooper showed that if a couple of electrons with an attractive interaction (due to phonons) is added outside, but near, the Fermi surface, it forms a new state with energy lower than $2\epsilon_F$.
The Schrödinger equation of 2 extra electrons will be

$$\left[-\frac{\hbar^2}{2m}\left(\nabla_1^2 + \nabla_2^2\right) + U(\mathbf{r}_2 - \mathbf{r}_1)\right]\Psi(\mathbf{r}_1, \mathbf{r}_2) = E\Psi(\mathbf{r}_1, \mathbf{r}_2), \tag{1.1}$$

$$\begin{aligned}\Psi(\mathbf{r}_1,\mathbf{r}_2) &= \langle \mathbf{r}_1,\mathbf{r}_2|\Psi_{12}\rangle \\ |\Psi_{12}\rangle &= \sum_{\mathbf{k}_1,\mathbf{k}_2} \alpha(\mathbf{k}_1,\mathbf{k}_2) c^\dagger_{\mathbf{k}_1} c^\dagger_{\mathbf{k}_2}|\Psi_0\rangle \\ \alpha(\mathbf{k}_1,\mathbf{k}_2) &= \frac{1}{V}\exp[-i(\mathbf{k}_1\cdot\mathbf{r}_1+\mathbf{k}_2\cdot\mathbf{r}_2)],\end{aligned} \tag{1.2}$$

where m is the electron mass, $\mathbf{r}_1, \mathbf{r}_2$ are the positions of the two electrons, $\mathbf{k}_1, \mathbf{k}_2$ are their momenta. $\alpha(\mathbf{k}_1, \mathbf{k}_2)$ is the coefficient of the Fourier expansion.

Since the pair is taken near the Fermi surface, the energy of the two electrons will be confined in a small interval $[\epsilon_F, \epsilon_F + \hbar\omega_{\mathbf{q}}]$. $\omega_{\mathbf{q}}$ is the frequency of the phonon exchanged by the two electrons and it can never be larger than the Debye frequency ω_D. If we consider the center of mass of the couple with momentum $\mathbf{K} = \mathbf{k}_1 + \mathbf{k}_2$ we can see that only some momenta $\mathbf{k}_1, \mathbf{k}_2$ give a non zero contribution to $|\Psi_{12}\rangle$, those whose sum is $\mathbf{K}$. If we try maximize the number of combinations that give $\mathbf{K}$ total momentum, we see that it happens when $\mathbf{K} = 0$, i.e. when $\mathbf{k}_2 = -\mathbf{k}_1$, hence from here on we drop the momentum subscript. From experimental observations (see Bordoloi et al. (2022)) it is known that the two electrons forming the pair have opposite spin, hence they form a singlet. The couple wavefunction in real space can be written as a plane wave expansion

$$\Psi(\mathbf{r}_1 - \mathbf{r}_2) = \frac{1}{V}\sum_{\mathbf{k}} \alpha_{\mathbf{k}} e^{i\mathbf{k}\cdot\mathbf{r}_1} e^{-i\mathbf{k}\cdot\mathbf{r}_2}; \tag{1.3}$$

then by defining $\mathbf{r} = \mathbf{r}_1 - \mathbf{r}_2$ we get

$$\Psi(\mathbf{r}) = \frac{1}{V}\sum_{\mathbf{k}} \alpha_{\mathbf{k}} e^{i\mathbf{k}\cdot\mathbf{r}}. \tag{1.4}$$

By plugging this expression into 1.1, multiplying both sides by $e^{-i\mathbf{k}'\cdot\mathbf{r}}$ and integrating over $\mathbf{r}$ the Schrödinger equation becomes

$$V[2E_{\mathbf{k}} - E]\alpha_{\mathbf{k}} + \sum_{\mathbf{k}'} U(\mathbf{k}' - \mathbf{k})\alpha_{\mathbf{k}'} = 0 \tag{1.5}$$

, where

$$\begin{aligned}U(\mathbf{k}' - \mathbf{k}) &= \int d\mathbf{r} U(\mathbf{r}) e^{i(\mathbf{k}-\mathbf{k}')\cdot\mathbf{r}} \\ E_{\mathbf{k}} &= \frac{\hbar^2\mathbf{k}^2}{2m}.\end{aligned} \tag{1.6}$$

As pointed out by Cooper (Cooper (1956)) the interaction between the electrons is attractive and can be taken as constant since $\hbar\omega << E_F$ (where E_F is the Fermi energy); therefore 1.5 can be approximated with

$$V\alpha_{\mathbf{k}} = \frac{U}{2E_{\mathbf{k}} - E}\sum_{\mathbf{k}'} \alpha_{\mathbf{k}'}. \tag{1.7}$$

Now by summing both sides over $\mathbf{k}$ we get

$$\sum_{\mathbf{k}} \frac{1}{2E_{\mathbf{k}} - E} = \frac{V}{U}. \tag{1.8}$$

The first singularity of this function occurs when $E = 2E_F$, meaning that the lowest eigenvalue E_0 of the ground state is reached before the singularity; hence we can define the binding energy of

the pair as $\Delta = 2E_F - E_0$ Using expression 1.8 we can rewrite the eigenvalue equation as

$$1 = U \int_{\epsilon_F}^{\epsilon_F + \hbar\omega_D} \frac{g(\epsilon)}{2\epsilon - E_0} d\epsilon, \tag{1.9}$$

where $g(\epsilon)$ is the density of states Since the energy interval over which we are integrating is very thin (i.e. $\hbar\omega_D << E_F$) we can approximate the density of states with its value at the Fermi energy (i.e.$g(\epsilon_F)$) and the integral yields:

$$\frac{e^{\frac{2}{Ug(E_F)}} - 1}{2\hbar\omega_D} = \frac{1}{\Delta}. \tag{1.10}$$

Expanding the exponential up to first order we obtain the binding energy of the Cooper pair

$$\Delta \approx 2\hbar\omega_D e^{-\frac{2}{Ug(E_F)}}. \tag{1.11}$$

We can see from the previous expression that the binding energy is small with respect to the Debye energy $\hbar\omega_D$, but it is positive; hence we found out that the presence of an attractive interaction makes the Fermi sphere unstable, while it favors a state in which electrons are paired.

1.3.2 Ground state

In 1957 Bardeen, Cooper and Schriffer proposed a variational wavefunction to describe a superconducting ground state

$$|\Psi_{BCS}\rangle = \prod_{\mathbf{k}} (u_{\mathbf{k}} + v_{\mathbf{k}} c^\dagger_{\mathbf{k},\uparrow} c^\dagger_{-\mathbf{k},\downarrow})|0\rangle, \tag{1.12}$$

which consists of a superposition of states with different numbers of Cooper pairs. The operator $c^\dagger_{\mathbf{k}\sigma}$ creates an electron with momentum $\mathbf{k}$ and spin σ in the empty state $|0\rangle$. Due to the Cooper theorem discussed in Sec.1.3.1 we already know that the two electrons forming the pair have opposite spins and momenta; $u_{\mathbf{k}}$ and $v_{\mathbf{k}}$ are variational parameters. Without loss of generality we can take the constraint $|u_{\mathbf{k}}|^2 + |v_{\mathbf{k}}|^2 = 1$, that allow us to define: $|u_{\mathbf{k}}|^2$ as the probability for a pair not to be occupied and $|v_{\mathbf{k}}|^2$ as the probability for a pair to be occupied. This condition allows the wavefunction to be properly renormalized, i.e:

$$\begin{aligned}\langle \Psi_{BCS}|\Psi_{BCS}\rangle &= \langle 0| \prod_{\mathbf{k}} \prod_{\mathbf{k}'} u^*_{\mathbf{k}} u_{\mathbf{k}'} + u^*_{\mathbf{k}} v_{\mathbf{k}'} c^\dagger_{\mathbf{k}',\uparrow} c^\dagger_{-\mathbf{k}',\downarrow} + v^*_{\mathbf{k}} u_{\mathbf{k}'} c_{-\mathbf{k},\downarrow} c_{\mathbf{k},\uparrow} + v^*_{\mathbf{k}} v_{\mathbf{k}'} c_{-\mathbf{k},\downarrow} c_{\mathbf{k},\uparrow} c c^\dagger_{\mathbf{k}',\uparrow} c^\dagger_{-\mathbf{k}',\downarrow} |0\rangle = \\ &= \prod_{\mathbf{k}} (|u_{\mathbf{k}}|^2 + |v_{\mathbf{k}}|^2).\end{aligned} \tag{1.13}$$

It is also important to highlight that since the BCS state does not have a fixed number of particles, it is useful to switch to the grand canonical ensamble with the constraint $\langle \Psi_{BCS}|N_p|\Psi_{BCS}\rangle = N$, where N is the average number of pairs and $N_p = \sum_{\mathbf{k}} (c^\dagger_{\mathbf{k},\uparrow} c_{\mathbf{k},\uparrow} + c^\dagger_{-\mathbf{k},\downarrow} c_{-\mathbf{k},\downarrow})$ is the corresponding operator. Now we can introduce a chemical potential μ and a new Hamiltonian $\mathcal{H}_{\mathcal{BCS}} = H - \mu N$ where H is the Hamiltonian of a system with an attractive interaction. The BCS Hamiltonian reads:

$$\mathcal{H}_{\mathcal{BCS}} = \sum_{\mathbf{k}} \epsilon_{\mathbf{k}} (c^\dagger_{\mathbf{k},\uparrow} c_{\mathbf{k},\uparrow} + c^\dagger_{-\mathbf{k},\downarrow} c_{-\mathbf{k},\downarrow}) + \sum_{\mathbf{k},\mathbf{k}'} U_{\mathbf{k},\mathbf{k}'} c^\dagger_{\mathbf{k},\uparrow} c^\dagger_{-\mathbf{k},\downarrow} c_{-\mathbf{k}',\downarrow} c_{\mathbf{k}',\uparrow}, \tag{1.14}$$

where $\epsilon_{\mathbf{k}} = \frac{\hbar^2\mathbf{k}^2}{2m} - \mu$ and $U_{\mathbf{k},\mathbf{k}'}$ is the attractive interaction. Using the following average values

$$\begin{aligned} \langle\Psi_{BCS}|c^\dagger_{\mathbf{k},\uparrow}c_{\mathbf{k},\uparrow}|\Psi_{BCS}\rangle &= v^2_{\mathbf{k}} \\ \langle\Psi_{BCS}|c^\dagger_{\mathbf{k},\uparrow}c^\dagger_{-\mathbf{k},\downarrow}|\Psi_{BCS}\rangle &= u_{\mathbf{k}}v_{\mathbf{k}}, \end{aligned} \tag{1.15}$$

and the fact that $v^2_{\mathbf{k}} + u^2_{\mathbf{k}} = 1$ we can calculate the average energy W_{BCS} as:

$$\begin{aligned} W_{BCS} &= \langle\Psi_{BCS}|\mathcal{H}_{\mathcal{BCS}}|\Psi_{BCS}\rangle \\ &= 2\sum_{\mathbf{k}}\epsilon_{\mathbf{k}}v^2_{\mathbf{k}} + \sum_{\mathbf{k},\mathbf{k}'}U_{\mathbf{k},\mathbf{k}'}u_{\mathbf{k}}v_{\mathbf{k}}u_{\mathbf{k}'}v_{\mathbf{k}'} \\ &= 2\sum_{\mathbf{k}}\epsilon_{\mathbf{k}}\sin\theta_{\mathbf{k}}{}^2 + \frac{1}{4}\sum_{\mathbf{k},\mathbf{k}'}U_{\mathbf{k},\mathbf{k}'}\sin 2\theta_{\mathbf{k}}\sin 2\theta_{\mathbf{k}'}, \end{aligned} \tag{1.16}$$

where $\theta_{\mathbf{k}}$ is such that $u_{\mathbf{k}} = \cos\theta_{\mathbf{k}}$ and $v_{\mathbf{k}} = \sin\theta_{\mathbf{k}}$. Now if we minimize W_{BCS}, i.e. calculate the its derivative with respect to θ_k and set it to zero, we get

$$2\epsilon_{\mathbf{k}}\sin 2\theta_{\mathbf{k}} + \sum_{\mathbf{k}}U_{\mathbf{k},\mathbf{k}'}\cos 2\theta_{\mathbf{k}}\sin 2\theta_{\mathbf{k}'} = 0. \tag{1.17}$$

Substituting back $u_{\mathbf{k}}$ and $v_{\mathbf{k}}$ we get

$$2\epsilon_{\mathbf{k}}u_{\mathbf{k}}v_{\mathbf{k}} + \sum_{\mathbf{k}'}U_{\mathbf{k},\mathbf{k}'}(u^2_{\mathbf{k}} - v^2_{\mathbf{k}})u_{\mathbf{k}'}v_{\mathbf{k}'} = 0. \tag{1.18}$$

Now by defining the gap parameter $\Delta_{\mathbf{k}} = \sum_{\mathbf{k}'}U_{\mathbf{k},\mathbf{k}'}u_{\mathbf{k}'}v_{\mathbf{k}'}$ and taking into account the condition $u^2_{\mathbf{k}} + v^2_{\mathbf{k}} = 1$ we get:

$$\begin{cases} 2\epsilon_{\mathbf{k}}u_{\mathbf{k}}v_{\mathbf{k}} - \Delta_{\mathbf{k}}(u^2_{\mathbf{k}} - v^2_{\mathbf{k}}) = 0 \\ u^2_{\mathbf{k}} + v^2_{\mathbf{k}} = 1, \end{cases} \tag{1.19}$$

from which we can obtain the variational parameters' expressions:

$$u^2_{\mathbf{k}} = \frac{1}{2}\left[1 + \frac{\epsilon_{\mathbf{k}}}{\sqrt{\epsilon^2_{\mathbf{k}} + \Delta^2_{\mathbf{k}}}}\right] \qquad\qquad v^2_{\mathbf{k}} = \frac{1}{2}\left[1 - \frac{\epsilon_{\mathbf{k}}}{\sqrt{\epsilon^2_{\mathbf{k}} + \Delta^2_{\mathbf{k}}}}\right]$$

Finally we can use these in the definition of $\Delta_{\mathbf{k}}$ and obtain:

$$\Delta_{\mathbf{k}} = -\frac{1}{2}\sum_{\mathbf{k}'}U_{\mathbf{k},\mathbf{k}'}\frac{\Delta_{\mathbf{k}'}}{\sqrt{\epsilon^2_{\mathbf{k}'} + \Delta^2_{\mathbf{k}'}}} \tag{1.20}$$

which is a self consistent equation for the gap parameter.

1.3.3 Mean field BCS: T = 0 case

The BCS Hamiltonian stated in Eq.1.14 is impossible to diagonalize directly; hence we will try a mean field approach. First we need to insert the fluctuations, therefore let us introduce $a_{\mathbf{k}} = \langle\Psi_{BCS}|c_{\mathbf{k},\uparrow}c_{-\mathbf{k},\downarrow}|\Psi_{BCS}\rangle$ (assume $a_{\mathbf{k}}$ real for simplicity), such that $c^\dagger_{\mathbf{k},\uparrow}c^\dagger_{-\mathbf{k},\downarrow} = a_{\mathbf{k}} + (c^\dagger_{\mathbf{k},\uparrow}c^\dagger_{-\mathbf{k},\downarrow} - a_{\mathbf{k}})$. If we insert $a_{\mathbf{k}}$ in Eq.1.14 and consider terms up to first order in $a_{\mathbf{k}}$ we are left with:

$$\begin{aligned} \mathcal{H}_{\mathcal{BCS}} &= \sum_{\mathbf{k}}\epsilon_{\mathbf{k}}(c^\dagger_{\mathbf{k},\uparrow}c_{\mathbf{k},\uparrow} + c^\dagger_{-\mathbf{k},\downarrow}c_{-\mathbf{k},\downarrow}) - \sum_{\mathbf{k}}\Delta_{\mathbf{k}}(c_{-\mathbf{k},\downarrow}c_{\mathbf{k},\uparrow} + c^\dagger_{\mathbf{k},\uparrow}c^\dagger_{-\mathbf{k},\downarrow}) + \sum_{\mathbf{k}}\Delta_{\mathbf{k}}a_{\mathbf{k}} \\ \Delta_{\mathbf{k}} &= \sum_{\mathbf{k}'}U_{\mathbf{k},\mathbf{k}'}a_{\mathbf{k}'}, \end{aligned} \tag{1.21}$$

which now is quadratic and can be diagonalized via a Bogoljubov transformation. We introduce the operators $\gamma_{\mathbf{k},\sigma}$ and $\gamma^\dagger_{\mathbf{k},\sigma}$ in such a way that

$$\begin{aligned} c_{\mathbf{k},\uparrow} &= u_{\mathbf{k}}\gamma_{\mathbf{k},\uparrow} + v_{\mathbf{k}}\gamma^\dagger_{-\mathbf{k},\downarrow} \\ c^\dagger_{\mathbf{k},\uparrow} &= u_{\mathbf{k}}\gamma^\dagger_{\mathbf{k},\uparrow} + v_{\mathbf{k}}\gamma_{-\mathbf{k},\downarrow} \\ c_{-\mathbf{k},\downarrow} &= u_{\mathbf{k}}\gamma_{-\mathbf{k},\downarrow} - v_{\mathbf{k}}\gamma^\dagger_{\mathbf{k},\uparrow} \\ c^\dagger_{-\mathbf{k},\downarrow} &= u_{\mathbf{k}}\gamma^\dagger_{-\mathbf{k},\downarrow} - v_{\mathbf{k}}\gamma_{\mathbf{k},\uparrow}. \end{aligned} \tag{1.22}$$

Anti-commutation relations are preserved due to the condition $u^2_{\mathbf{k}} + v^2_{\mathbf{k}} = 1$ fixed above. Rewriting the Hamiltonian we get

$$\begin{aligned} \mathcal{H}_{\mathcal{BCS}} = &\sum_{\mathbf{k}} [\epsilon_{\mathbf{k}}(u^2_{\mathbf{k}} - v^2_{\mathbf{k}}) + 2\Delta_{\mathbf{k}} u_{\mathbf{k}} v_{\mathbf{k}}](\gamma^\dagger_{\mathbf{k},\uparrow}\gamma_{\mathbf{k},\uparrow} + \gamma^\dagger_{-\mathbf{k},\downarrow}\gamma_{-\mathbf{k},\downarrow}) + \\ &+ \sum_{\mathbf{k}} [2\epsilon_{\mathbf{k}} u_{\mathbf{k}} v_{\mathbf{k}} - \Delta_{\mathbf{k}}(u^2_{\mathbf{k}} - v^2_{\mathbf{k}})](\gamma^\dagger_{\mathbf{k},\uparrow}\gamma^\dagger_{-\mathbf{k},\downarrow} + \gamma_{-\mathbf{k},\downarrow}\gamma_{\mathbf{k},\uparrow}) + \\ &+ const. \end{aligned} \tag{1.23}$$

The first term is diagonal in the γ operators while the second is not. In order to solve this problem we impose that $2\epsilon_{\mathbf{k}} u_{\mathbf{k}} v_{\mathbf{k}} - \Delta_{\mathbf{k}}(u^2_{\mathbf{k}} - v^2_{\mathbf{k}}) = 0$ which paired with $u^2_{\mathbf{k}} + v^2_{\mathbf{k}} = 1$ yields the same conditions for $u_{\mathbf{k}}$ and $v_{\mathbf{k}}$ found before. Upon inserting these relations in 1.23 we are left with

$$\mathcal{H}_{\mathcal{BCS}} = \sum_{\mathbf{k}} \sqrt{\epsilon^2_{\mathbf{k}} + \Delta^2_{\mathbf{k}}}(\gamma^\dagger_{\mathbf{k},\uparrow}\gamma_{\mathbf{k},\uparrow} + \gamma^\dagger_{-\mathbf{k},\downarrow}\gamma_{-\mathbf{k},\downarrow}). \tag{1.24}$$

If we restrain ourselves at small energy intervals we can approximate $\Delta_{\mathbf{k}}$ with Δ_0 and observe that the spectrum of the quasi-particles created by γ is gapped, meaning that the ground state is protected at low (but finite) temperatures.

1.3.4 Mean field BCS: T > 0 case

Now we want to extend the previous approach to higher temperatures, to do so we define $a_{\mathbf{k}} = \langle c^\dagger_{\mathbf{k}\uparrow} c^\dagger_{-\mathbf{k}\uparrow}\rangle_T$ which indicates the average value of the fluctuations at temperature T. As before, we assume $a_{\mathbf{k}}$ to be real. Using a Bogoljubov transformation, we have that

$$\begin{aligned} \langle c^\dagger_{\mathbf{k}\uparrow} c^\dagger_{-\mathbf{k}\uparrow}\rangle_T &= u_{\mathbf{k}} v_{\mathbf{k}} \langle 1 - \gamma^\dagger_{-\mathbf{k}\downarrow}\gamma_{-\mathbf{k}\downarrow} - \gamma^\dagger_{\mathbf{k}\uparrow}\gamma_{\mathbf{k}\uparrow}\rangle_T \\ &= u_{\mathbf{k}} v_{\mathbf{k}} [1 - 2f(w_{\mathbf{k}})], \end{aligned} \tag{1.25}$$

where $f(w_{\mathbf{k}})$ is the Fermi-Dirac distribution for the quasi-particles and $w_{\mathbf{k}} = \sqrt{\epsilon^2_{\mathbf{k}} + \Delta^2_{\mathbf{k}}}$. Using the identity:

$$1 - 2f(w_{\mathbf{k}}) = \tanh \frac{\beta\omega_{\mathbf{k}}}{2}, \tag{1.26}$$

a self-consistent equation for the gap parameter is obtained:

$$\Delta_{\mathbf{k}} = -\frac{1}{2}\sum_{\mathbf{k}'} U_{\mathbf{k},\mathbf{k}'} \frac{\Delta_{\mathbf{k}'}}{\sqrt{\epsilon^2_{\mathbf{k}'} + \Delta^2_{\mathbf{k}'}}} \tanh \frac{\beta\sqrt{\epsilon^2_{\mathbf{k}'} + \Delta^2_{\mathbf{k}'}}}{2}. \tag{1.27}$$

If now we consider an interaction such that $U_{\mathbf{k},\mathbf{k}'} = -\frac{U}{V}$ when $-\hbar\omega_D < \epsilon_{\mathbf{k}} < \hbar\omega_D$ and 0 otherwise, and we transform the sum in 1.27 into an integral, we are left with:

$$1 = \frac{1}{2} U g(\epsilon_F) \int_{-\hbar\omega_D}^{\hbar\omega_D} \frac{d\epsilon}{\sqrt{\epsilon^2 + \Delta^2}} \tanh \frac{\beta\sqrt{\epsilon^2 + \Delta^2}}{2}, \tag{1.28}$$

where we approximated the density of states with its value at the Fermi energy since the energy interval is small. In the $T \to 0$ limit the hyperbolic tangent goes to 1 and we recover the $T = 0$ case discussed above. It is also evident that if T increases the gap Δ has to become smaller to maintain the integral constant, meaning that for some value of T (T_C i.e. the critical temperature) the gap closes. Solving the integral for T_C yields

$$k_B T_C = \frac{2e^{\gamma}}{\pi} \hbar\omega_D e^{-\frac{1}{U g(\epsilon_F)}}, \tag{1.29}$$

where γ is Euler's number and k_B is Boltzmann's constant.

1.4 High-temperature superconductivity

The electronic state of many materials with partially filled d-shells, such as transition metal oxides, is characterized by strong correlations. Materials with such correlations display fascinating properties such as metal-insulator transitions and high-temperature superconductivity. The presence of strong correlations makes clear that the BCS theory is not adequate to describe the high- temperature superconductivity, indeed the critical temperature predicted by BCS calculations is lower than the one measured in experiments. It has been argued that such difference between theoretical calculations and experiments is due to the fact that the superconductivity does not come from the fact that electrons are coupled by a phonon; instead, it might come from spin fluctuations of the electrons. Indeed it has been observed that superconductivity emerges when the parent compound is taken out of half filling by *doping* it (i.e. charge carriers are injected in the system). Therefore, since parent compounds of many transition metal oxides are Mott insulators, there is a correlation between high temperature superconductivity and Mott physics.

Cuprates are one of the families of high-temperature superconductors; however, they feature a fascinating characteristic, i.e. having a single partially filled electronic band at the Fermi level. Instead other transition metal oxides, such as iron-based superconductors, are multi-band materials. In multi-band materials, it has recently been highlighted the effect of Hund's coupling. Hund's coupling is the exchange interaction between electrons in the same atom; its effect is to lower the cost in Coulomb energy when placing the electrons in different orbitals with parallel spin. This shakes the idea of Mottness being the sole origin of strong correlations, and suggests that there is another class of strongly correlated materials, which have been named Hund's metals. For multi-orbital shells, such as those of IBSs, Hund's coupling lowers the effect of fluctuations favoring states with the highest possible spin on each transition metal ion (De'Medici and Capone (2017)).

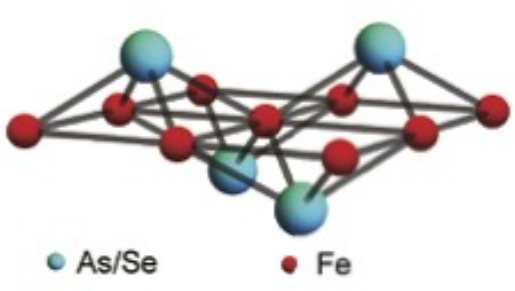

Figure 1.1: Schematic crystal structure of a FeAs/FeSe plane, displaying the Fe plane with the As/Se atoms alternating above and below the centers of the squares. Figure reproduced from Fernandes and Chubukov (2016).

1.4.1 Iron-based superconductors

The discovery of a rich family of iron-based superconductors such as LaFeAsO, $BaFe_2As_2$ (see fig.1.2), NaFeAs, FeSe opened a new route for studying high-temperature superconductivity. These materials are organized in layers of FeAs where Fe atoms form a square lattice. Usually the parent compound of such materials (i.e. the undoped compound) is a magnetically ordered metal, where the magnetic order is in such a way that electrons are ferromagnetically aligned in one direction and antiferromagnetically aligned in the other.
The fact that the parent compound is a metal is due to the fact that low-energy states arise from Fe^{2+}, which is in a $3d^6$ configuration. Such configuration involves five orbitals d_{xz},d_{yz},d_{xy},$d_{x^2-y^2}$ and $d_{3z^2-r^2}$ (Fernandes and Chubukov (2016)).
In a crystal these five levels are split in two subsets: d_{xz},d_{yz},d_{xy} for t_{2g} and $d_{x^2-y^2}$,$d_{3z^2-r^2}$ for e_g; however, the splitting between the two subsets is not large enough to justify a priori to limit the study to just a subset of orbitals; hence we have to build a model taking into account all five d orbitals (Fernandes and Chubukov (2016)).

As we can see in figure 1.1, the crystalline structure is made up of a square lattice of iron atoms, while As/Se atoms alternate between those above and below the Fe squares. A consequence of that is the fact that the crystal structure is an hybrid between a tetrahedral and a tetragonal one, making difficult to discern which group of orbitals plays a major role in determining the Fermi surface.

Nevertheless, calculations (Fernandes and Chubukov (2016)) showed that the main contributions to the Fermi surface are given by the three orbitals in the t_{2g} subset, hence a simplified model with three orbitals has been proposed and it has been shown(Daghofer et al. (2010)) that in the weak-coupling limit it reproduces the Fermi surface correctly. Another possibility is to construct a two-orbital model observing the fact that the d_{xy} orbital can be hybridized with the d_{xz} orbital(Raghu et al. (2010)). The order parameter for superconductivity in the model is the superconductive

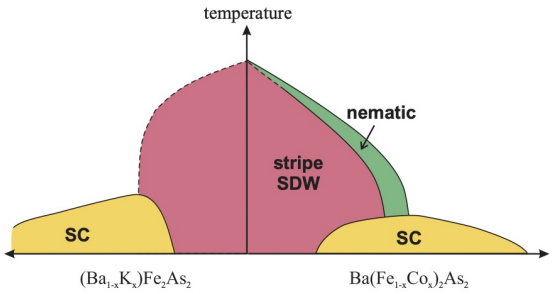

Figure 1.2: Phase diagram of Co-doped (el-doped) and K-doped (hole-doped) $BaFe_2As_2$, displaying nematic and spin density wave (SDW) order and superconductivity. Figure reproduced from Fernandes and Chubukov (2016).

gap (see eq.1.20) $\Delta_{SC}^{\alpha,\beta}(\mathbf{k})$ (where α and β are orbital indices). In general, the dependence of the gap from $\mathbf{k}$ is not trivial, since it reflects the lattice symmetries. Therefore, by studying the gap symmetries we can classify different types of superconductivity. As an example: if the gap is such that it is positive at $(0,0)$ and (π,π), while being negative at $(\pi,0)$ and $(0,\pi)$, we have an s-wave superconductor with an $s^{\pm}$ symmetry, which is the symmetry usually considered for IBS.
Regarding IBS a combination between weak- and strong-coupling regime is better suited to describe such materials. A possible explanation of that is the presence of a Mott-transition featuring orbital selectivity(De'Medici and Capone (2017)); in such a condition the Coulomb interaction may be different for different orbitals due to the Hund's coupling, resulting in a mixed weak-/strong-coupling regime.

1.4.2 Cuprate superconductors

Cuprates are a family of superconductors characterized by a crystalline structure made of CuO_2 planes separated by layers of other atoms such as: Ba,La,O and many others. Unlike IBSs, where the parent compounds are metals, parent compounds of cuprates are Mott insulators.
Low-energy properties of cuprates are determined by Cu^{2+} ions, which are in a $3d^9$ configuration. This configuration contains just one orbital, $d_{x^2-y^2}$, meaning that a single-band model is enough to describe the system.
The crystalline structure of cuprates makes clear that the correct regime to describe them is the strong-coupling one, since there is a strong on-site repulsion.

Chapter 2

Hubbard model

The Hubbard model was introduced in by Hubbard, Gutzwiller and Kanamori. It gives a simple description of electrons interacting with each other in a lattice. In order to derive the Hubbard Hamiltonian we start from the many-body Hamiltonian for N interacting electrons in a periodic potential generated by a lattice with L sites within the Born-Oppenheimer approximation, which allows us to consider atomic nuclei as nearly fixed with respect to the electrons, since they are much more massive than electrons(Giuliani and Vignale (2005)):

$$\begin{aligned}\mathcal{H} &= \mathcal{H}_{kin} + \mathcal{H}_{el-ion} + \mathcal{H}_{int} \\ &= -\frac{\hbar^2}{2m}\sum_{n=1}^{N}\nabla_n^2 + \sum_{n=1}^{N}\sum_{i=1}^{L} V_1(\mathbf{x}_n - \mathbf{R}_i) + \frac{1}{2}\sum_{n\neq n'} V_2(\mathbf{x}_n - \mathbf{x}_{n'}),\end{aligned} \tag{2.1}$$

where x_n is the position of the n-th electron, R_i is the position of the i-th ion, V_1 is the electron-ion interaction and V_2 is the electron-electron interaction.

Since we are interested in studying the behavior of each electron we look for a basis of single-particle wavefunctions for each site R of the lattice, $\Phi_{\alpha,\mathbf{R}}(\mathbf{x},\sigma)$ (α is the orbital index). Due to the fact that the Hamiltonian (2.1) is spin independent we can factorize the wavefunction in a spatial dependent part($\phi_{\alpha,\mathbf{R}}(\mathbf{x})$) and a spin dependent part (ω_σ), hence $\Phi_{\alpha,\mathbf{R}}(\mathbf{x},\sigma) = \phi_{\alpha,\mathbf{R}}(\mathbf{x})\omega_\sigma$. In the case of strongly correlated materials the spatial part is given by localized Wannier orbitals(De'Medici and Capone (2017)) satisfying the conditions:

$$\begin{aligned}\int d\mathbf{x}\phi^*_{\alpha,\mathbf{R}_1}(\mathbf{x})\phi_{\beta,\mathbf{R}_2}(\mathbf{x}) &= \delta_{\alpha,\beta}\delta_{\mathbf{R}_1,\mathbf{R}_2} \\ \sum_{\alpha,\mathbf{R}} \phi^*_{\alpha,\mathbf{R}}(\mathbf{x})\phi_{\alpha,\mathbf{R}}(\mathbf{y}) &= \delta(\mathbf{x}-\mathbf{y}).\end{aligned} \tag{2.2}$$

In this basis the Fermi field operator for electrons with spin σ in real space reads:

$$\Psi_\sigma(\mathbf{x}) = \sum_{\alpha,\mathbf{R}} \phi_{\alpha,\mathbf{R}}(\mathbf{x})c_{\alpha,\mathbf{R},\sigma}, \tag{2.3}$$

where $\Psi_\sigma(\mathbf{x})^\dagger = (\Psi_\sigma(\mathbf{x}))^\dagger$.

Now we can obtain the Hamiltonian (2.1) in second quantization form. First we deal with the non

interacting part:

$$\mathcal{H}_0 = \mathcal{H}_{kin} + \mathcal{H}_{el-ion} = \sum_\sigma \int d\mathbf{x} \Psi^\dagger_\sigma(\mathbf{x}) \left[-\frac{\hbar^2}{2m}\nabla^2 + \sum_i V_1(\mathbf{x} - \mathbf{R}_i) \right] \Psi_\sigma(\mathbf{x}). \tag{2.4}$$

If we define the matrix element $t^{\alpha,\beta}_{R_1,R_2}$ as:

$$\begin{aligned} t^{\alpha,\beta}_{R_1,R_2} &= \int d\mathbf{x} \phi^*_{\alpha,\mathbf{R}_1}(\mathbf{x}) \left[-\frac{\hbar^2}{2m}\nabla^2 + \sum_i V_1(\mathbf{x} - \mathbf{R}_i) \right] \phi_{\beta,\mathbf{R}_2}(\mathbf{x}) \\ t^{\alpha,\beta}_{R_1,R_2} &= (t^{\beta,\alpha}_{R_2,R_1})^*, \end{aligned} \tag{2.5}$$

and use the expansion of $\Psi_\sigma(\mathbf{x})$ in Wannier functions we get:

$$\mathcal{H}_0 = \sum_\sigma \sum_{\alpha,\beta} \sum_{\mathbf{R_1},\mathbf{R_2}} t^{\alpha,\beta}_{R_1,R_2} c^\dagger_{\alpha,\mathbf{R_1},\sigma} c_{\beta,\mathbf{R_2},\sigma}. \tag{2.6}$$

Taking the Fourier transform of the Fermi operator we get:

$$\mathcal{H}_0 = \frac{1}{L} \sum_\sigma \sum_{\alpha,\beta} \sum_{\mathbf{R_1},\mathbf{R_2}} \sum_{\mathbf{q}_1,\mathbf{q}_2} e^{-i\mathbf{q}_1\cdot\mathbf{R}_1} e^{i\mathbf{q}_2\cdot\mathbf{R}_2} t^{\alpha,\beta}_{R_1,R_2} c^\dagger_{\alpha,\mathbf{q}_1,\sigma} c_{\beta,\mathbf{q}_2,\sigma}. \tag{2.7}$$

By using the definition of Kronecker delta and considering that in a translationally invariant lattice hoppings depend on the distance between the sites, we obtain:

$$\mathcal{H}_0 = \sum_\sigma \sum_{\alpha,\beta} \sum_{\mathbf{q}} t^{\alpha,\beta}_{\mathbf{q}} c^\dagger_{\alpha,\mathbf{q},\sigma} c_{\beta,\mathbf{q},\sigma}. \tag{2.8}$$

When treating the interaction part we get:

$$U^{\alpha,\beta,\gamma,\delta}_{\mathbf{R}_1,\mathbf{R}_2,\mathbf{R}_3,\mathbf{R}_4} = \int d\mathbf{x} d\mathbf{y} \phi^*_{\alpha,\mathbf{R}_1}(\mathbf{x}) \phi^*_{\beta,\mathbf{R}_2}(\mathbf{y}) V_2(\mathbf{x}-\mathbf{y}) \phi_{\gamma,\mathbf{R}_3}(\mathbf{y}) \phi_{\delta,\mathbf{R}_4}(\mathbf{x}), \tag{2.9}$$

where we used the same wavefunction factorization above. Now by using again the same factorization we obtain:

$$\mathcal{H}_{int} = \frac{1}{2} \sum_{\sigma,\sigma'} \sum_{\alpha,\beta,\gamma,\delta} \sum_{\mathbf{R}_1,\mathbf{R}_2,\mathbf{R}_3,\mathbf{R}_4} U^{\alpha,\beta,\gamma,\delta}_{\mathbf{R}_1,\mathbf{R}_2,\mathbf{R}_3,\mathbf{R}_4} c^\dagger_{\alpha,\mathbf{R}_1,\sigma} c^\dagger_{\beta,\mathbf{R}_2,\sigma'} c_{\gamma,\mathbf{R}_3,\sigma'} c_{\delta,\mathbf{R}_4,\sigma}. \tag{2.10}$$

2.1 Single-band Hubbard model

The simplest system described by the Hubbard model is one where we consider only one orbital per atom, i.e. one orbital per site. Despite being simple this model can capture the properties of materials where inter-orbital exchanges are negligible due to large gaps between the orbitals, like in the case of cuprates; hence we can neglect the orbital indices $\alpha, \beta, \gamma, \delta$. Another important approximation is the fact that we can neglect all the interaction terms except the on site ones, i.e. we consider only terms such that $U_{\mathbf{R}_1,\mathbf{R}_2,\mathbf{R}_3,\mathbf{R}_4} = U_{\mathbf{R},\mathbf{R},\mathbf{R},\mathbf{R}}$. In the simple case we are considering we can restrain to just nearest neighbor hoppings such that the energy minimum is in the Γ point, i.e. we take $t^{\alpha,\beta}_{\mathbf{R}_1,\mathbf{R}_2} = -t$, where sites $\mathbf{R}_1, \mathbf{R}_2$ are nearest neighbors. In the end, we are left with two parameters: the correlation strength U and the hopping t. The Hamiltonian reads:

$$\mathcal{H} = -t \sum_{\langle i,j\rangle,\sigma} c^\dagger_{i,\sigma} c_{j,\sigma} + h.c. + U \sum_i n_{i,\uparrow} n_{i,\downarrow}, \tag{2.11}$$

where $n_{i,\sigma} = c^{\dagger}_{i,\sigma} c_{i,\sigma}$ is the number operator and $\langle i, j \rangle$ indicates that sites i,j are nearest neighbors. Despite being so simple this model is quite hard to solve due to the fact that the hopping term is diagonal in the phase space while the correlation term is diagonal in the real space. Indeed it is solvable only in: one dimension with nearest neighbor hopping, infinite dimensions and in the $t = 0$, $U = 0$ limits.

The Mott insulator state arises at half-filling when $U \gtrsim W$, where W is the bandwidth of the model. Analytic calculations are possible only in the $U >> t$ limit, where we can treat the hopping as a perturbation.

2.2 Multi-band Hubbard model

For some materials, such as iron-based superconductors, the single orbital approximation does not yield the correct low-energy properties due to the fact that the crystalline structure does not present a sufficiently large gap between the orbitals, making necessary a multi-orbital approach.

The generalization of the single band model to a multi-band one is straightforward by taking into account intra-orbital and inter-orbital Coulumb repulsion, as well as Hund's coupling and pair hopping. We still consider only interaction terms such that $U_{\mathbf{R}_1,\mathbf{R}_2,\mathbf{R}_3,\mathbf{R}_4} = U_{\mathbf{R},\mathbf{R},\mathbf{R},\mathbf{R}}$. Now by taking into account the subset of orbitals mentioned in Sec.1.4.1 and selecting appropriate wavefunctions for the t_{2g} orbitals, $\phi_\alpha(\mathbf{x})$, we can write the interactions as follows(Georges et al. (2013)):

$$\begin{aligned} U &= \int d\mathbf{x} d\mathbf{y} \phi^*_\alpha(\mathbf{x}) \phi^*_\alpha(\mathbf{y}) V_2(\mathbf{x}-\mathbf{y}) \phi_\alpha(\mathbf{y}) \phi_\alpha(\mathbf{x}) \\ U' &= \int d\mathbf{x} d\mathbf{y} \phi^*_\alpha(\mathbf{x}) \phi^*_\beta(\mathbf{y}) V_2(\mathbf{x}-\mathbf{y}) \phi_\beta(\mathbf{y}) \phi_\alpha(\mathbf{x}) \\ J &= \int d\mathbf{x} d\mathbf{y} \phi^*_\alpha(\mathbf{x}) \phi^*_\beta(\mathbf{y}) V_2(\mathbf{x}-\mathbf{y}) \phi_\alpha(\mathbf{y}) \phi_\beta(\mathbf{x}) \\ J' &= \int d\mathbf{x} d\mathbf{y} \phi^*_\alpha(\mathbf{x}) \phi^*_\alpha(\mathbf{y}) V_2(\mathbf{x}-\mathbf{y}) \phi_\beta(\mathbf{y}) \phi_\beta(\mathbf{x}). \end{aligned} \tag{2.12}$$

In order, they are: intra-band Coulomb repulsion, inter-band Coulomb repulsion, Hund's coupling and pair-hopping.

Terms with three equal orbital indices vanish by symmetry(Georges et al. (2013)). If we choose real valued wavefunctions we can se that $J = J'$. Because there are no other interaction terms the

interaction Hamiltonian $\mathcal{H}_{int}$ (2.10) takes the form of the Kanamori Hamiltonian:

$$\begin{aligned}\mathcal{H}_K = & U \sum_{i,\alpha} n_{i,\alpha,\uparrow} n_{i,\alpha,\downarrow} \\ & + U' \sum_{i,\sigma \neq \sigma'} \sum_{\alpha<\beta} n_{i,\alpha,\sigma} n_{i,\beta,\sigma'} \\ & + (U' - J) \sum_{i,\sigma} \sum_{\alpha<\beta} n_{i,\alpha,\sigma} n_{i,\beta,\sigma} \\ & - J \sum_{i,\sigma \neq \sigma'} \sum_{\alpha<\beta} c^\dagger_{i,\alpha,\sigma} c_{i,\alpha,\sigma'} c^\dagger_{i,\beta,\sigma'} c_{i,\beta,\sigma} \\ & - J \sum_{i} \sum_{\alpha<\beta} (c^\dagger_{i,\alpha,\uparrow} c^\dagger_{i,\alpha,\downarrow} c_{i,\beta,\uparrow} c^\dagger_{i,\beta,\downarrow} + H.c.).\end{aligned} \tag{2.13}$$

In order to keep the Hamiltonian rotationally invariant (Georges et al. (2013)) we also have to take $U' = U - 2J$ yielding:

$$\begin{aligned}\mathcal{H}_K = & U \sum_{i,\alpha} n_{i,\alpha,\uparrow} n_{i,\alpha,\downarrow} \\ & + (U - 2J) \sum_{i,\sigma \neq \sigma'} \sum_{\alpha<\beta} n_{i,\alpha,\sigma} n_{i,\beta,\sigma'} \\ & + (U - 3J) \sum_{i,\sigma} \sum_{\alpha<\beta} n_{i,\alpha,\sigma} n_{i,\beta,\sigma} \\ & - J \sum_{i,\sigma \neq \sigma'} \sum_{\alpha<\beta} c^\dagger_{i,\alpha,\sigma} c_{i,\alpha,\sigma'} c^\dagger_{i,\beta,\sigma'} c_{i,\beta,\sigma} \\ & - J \sum_{i} \sum_{\alpha<\beta} (c^\dagger_{i,\alpha,\uparrow} c^\dagger_{i,\alpha,\downarrow} c_{i,\beta,\uparrow} c^\dagger_{i,\beta,\downarrow} + H.c.).\end{aligned} \tag{2.14}$$

Regarding the hopping term, for a simpler description, we choose to consider only nearest-neighbor hopping in order to get the energy minimum at the Γ point, i.e. $t^{\alpha,\beta}_{i,j} = -\delta_{\alpha,\beta} t$ (More general hoppings will be considered later). In the end for this three band example we get the following Hamiltonian:

$$\begin{aligned}\mathcal{H} = & -t \sum_{\langle i,j \rangle,\alpha,\sigma} c^\dagger_{i,\alpha,\sigma} c_{j,\alpha,\sigma} + h.c. \\ & + U \sum_{i,\alpha} n_{i,\alpha,\uparrow} n_{i,\alpha,\downarrow} \\ & + (U - 2J) \sum_{i,\sigma \neq \sigma'} \sum_{\alpha<\beta} n_{i,\alpha,\sigma} n_{i,\beta,\sigma'} \\ & + (U - 3J) \sum_{i,\sigma} \sum_{\alpha<\beta} n_{i,\alpha,\sigma} n_{i,\beta,\sigma} \\ & - J \sum_{i,\sigma \neq \sigma'} \sum_{\alpha<\beta} c^\dagger_{i,\alpha,\sigma} c_{i,\alpha,\sigma'} c^\dagger_{i,\beta,\sigma'} c_{i,\beta,\sigma} \\ & - J \sum_{i} \sum_{\alpha<\beta} (c^\dagger_{i,\alpha,\uparrow} c^\dagger_{i,\alpha,\downarrow} c_{i,\beta,\uparrow} c^\dagger_{i,\beta,\downarrow} + h.c.).\end{aligned} \tag{2.15}$$

If we repeat the same procedure as above for the e_g doublet we get a two bands Hamiltonian (Georges et al. (2013)):

$$\begin{aligned}\mathcal{H} = & -t \sum_{\langle i,j\rangle,\alpha,\sigma} c^{\dagger}_{i,\alpha,\sigma} c_{j,\alpha,\sigma} + h.c. \\ & + U \sum_{i,\alpha} n_{i,\alpha,\uparrow} n_{i,\alpha,\downarrow} + (U-2J) \sum_{i,\sigma\neq\sigma'} n_{i,1,\sigma} n_{i,2,\sigma'} \\ & + (U-3J) \sum_{i,\sigma} n_{i,1,\sigma} n_{i,2,\sigma} \\ & - J \sum_{i,\sigma\neq\sigma'} c^{\dagger}_{i,1,\sigma} c_{i,1,\sigma'} c^{\dagger}_{i,2,\sigma'} c_{i,2,\sigma} \\ & - J \sum_{i} (c^{\dagger}_{i,1,\uparrow} c^{\dagger}_{i,1,\downarrow} c_{i,2,\uparrow} c^{\dagger}_{i,2,\downarrow} + h.c.).\end{aligned} \tag{2.16}$$

2.3 Multi-band Hubbard models for iron-based superconductors

As we already discussed in section 1.4.1 the crystalline structure of iron-based superconductors is an hybrid of a tetrahedral and a tetragonal one; hence all five d orbitals have to be taken into account. The Hamiltonian for the kinetic energy in Fourier space reads:

$$\mathcal{H}_0 = \sum_{\alpha,\beta} (\epsilon_{\alpha,\beta} - \bar{\mu}\delta_{\alpha,\beta}) c^{\dagger}_{\alpha,\mathbf{q},\sigma} c_{\beta,\mathbf{q},\sigma}, \tag{2.17}$$

where $\bar{\mu}$ is the chemical potential and $\epsilon_{\alpha,\beta}$ are the tight-binding dispersion relations. Since we are considering a five-band Hamiltonian, $\mathcal{H}_0$ is obtained through the diagonalization of a 10x10 matrix which is an easy problem using computational methods. When we take into account the interactions, which in case of an iron-based superconductor are those described in section 2.2, the problem becomes extremely complicated to solve even with the aid of a computer; therefore some approximation is needed.

To solve the problem, simplified models have been proposed reducing the number of orbitals considered in the calculations such as a three orbital model(Fernandes and Chubukov (2016),Daghofer et al. (2010)) and a two orbital model (Fernandes and Chubukov (2016),Raghu et al. (2010)) yielding interesting results in predicting the properties of IBSs such as: Fermi surface, magnetic properties, superconductivity, orbital selectivity phenomena (Fernandes and Chubukov (2016), Raghu et al. (2010), Marino et al. (2024), de' Medici et al. (2014), Capone (2018)).

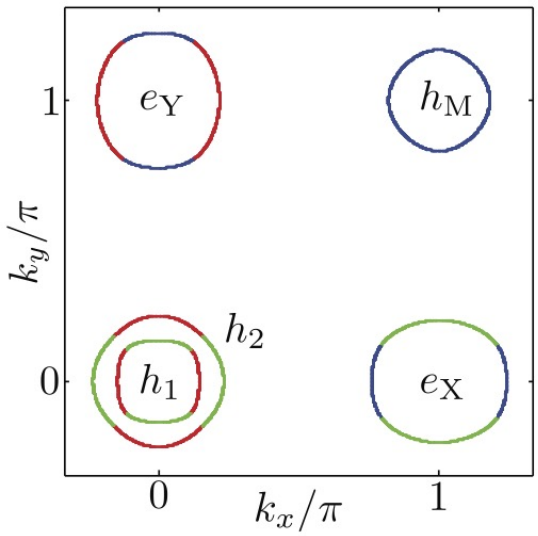

Figure 2.1: Fermi surface of the five-orbital model. Reproduced from Fernandes and Chubukov (2016)

2.3.1 Three orbital model

The three orbital model takes into account only the t_{2g} subset of orbitals: d_{xz}, d_{yz}, d_{xy}. The Hamiltonian for the kinetic energy is given by equation 2.8 with a more general hopping term:

$$\mathcal{H}_0 = \sum_{\mathbf{q},\alpha,\beta,\sigma} t_{\mathbf{q}}^{\alpha,\beta} c_{\mathbf{q},\alpha,\sigma}^{\dagger} c_{\mathbf{q},\beta,\sigma}. \tag{2.18}$$

As hoppings in Fourier space $t_{\mathbf{q}}^{\alpha,\beta}$ in $\mathcal{H}_0$ we take:

$$\begin{aligned}
t_{\mathbf{q}}^{xz,xz} &= 2t_2 \cos q_x + 2t_1 \cos q_y + 4t_3 \cos q_x \cos q_y \\
t_{\mathbf{q}}^{yz,yz} &= 2t_1 \cos q_x + 2t_2 \cos q_y + 4t_3 \cos q_x \cos q_y \\
t_{\mathbf{q}}^{xy,xy} &= 2t_5(\cos q_x + \cos q_y) + 4t_6 \cos q_x \cos q_y + \epsilon_{xy} \\
t_{\mathbf{q}}^{xz,yz} &= (t_{\mathbf{q}}^{yz,xz})^* = 4t_4 \sin q_x \sin q_y \\
t_{\mathbf{q}}^{xz,xy} &= (t_{\mathbf{q}}^{xy,xz})^* = 2it_7 \sin q_x + 4it_8 \sin q_x \sin q_y \\
t_{\mathbf{q}}^{yz,xy} &= (t_{\mathbf{q}}^{xy,yz})^* = 2it_7 \sin q_y + 4it_8 \sin q_x \sin q_y,
\end{aligned} \tag{2.19}$$

where t's are the inter- and intra-orbital hoppings (Marino et al. (2024)) and ϵ_{xy} is the crystal field splitting. The interaction part of the Hamiltonian is given by the Kanamori Hamiltonian 2.15 already discussed above.

The main issue with the three-orbital model is the fact that, due to the lack of hybridization with the e_g orbitals, the Fermi surface presents an anomalous hole-like pocket near the M point which indicates that all five orbitals are necessary to reproduce the correct geometry of the Fermi surface (Fernandes and Chubukov (2016)).

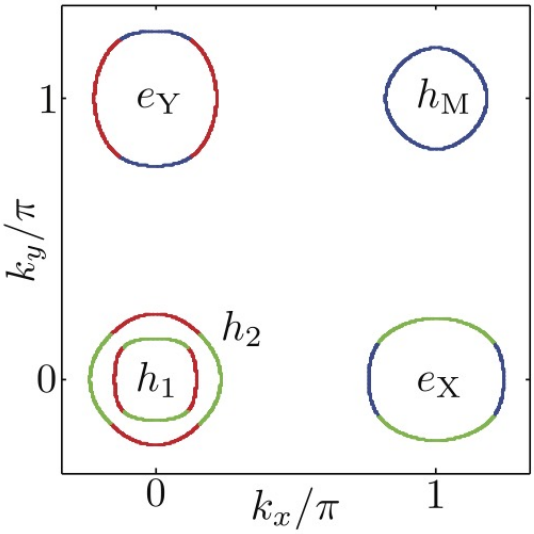

Figure 2.2: Fermi surface of the three-orbital model. Reproduced from Fernandes and Chubukov (2016)

2.3.2 Two orbital model

From band structure calculations (Raghu et al. (2010)) it is clear that the main contribution to the Fermi surface comes from the orbitals in the t_{2g} subset, however we can make the further approximation that the orbital d_{xy} can be substituted by hybridizing the d_{xz}, d_{yz} orbitals, yielding a model with just two orbitals per site.

The model Hamiltonian reads:

$$\mathcal{H} = \sum_{\mathbf{q},\alpha,\beta,\sigma} t_{\mathbf{q}}^{\alpha,\beta} c_{\mathbf{q},\alpha,\sigma}^{\dagger} c_{\mathbf{q},\beta,\sigma}. \tag{2.20}$$

It is the same as before with the difference that the orbital indices α, β run over just two orbitals. As a result of that the Hamiltonian is just a 3×3 matrix. As hoppings in the Fourier space we take:

$$\begin{aligned} t_{\mathbf{q}}^{xz,xz} &= 2t_2 \cos q_x + 2t_1 \cos q_y + 4t_3 \cos q_x \cos q_y \\ t_{\mathbf{q}}^{yz,yz} &= 2t_1 \cos q_x + 2t_2 \cos q_y + 4t_3 \cos q_x \cos q_y \\ t_{\mathbf{q}}^{xz,yz} &= (t_{\mathbf{q}}^{yz,xz})^* = 4t_4 \sin q_x \sin q_y. \end{aligned} \tag{2.21}$$

Again, the interaction part is given by the Kanamori Hamiltonian (see Eq.2.14).

This model might be too simplistic, indeed it does not only reproduce incorrectly the position of hole pockets of the Fermi surface but also violates the symmetries of the FeAs plane (Fernandes and Chubukov (2016)). Another issue with the two-orbital model, that has emerged from the results of this work (see chapter 4), is the fact that it does not present orbital selectivity when it is driven out of half-filling, meaning that the system described does not show superconductive correlations.

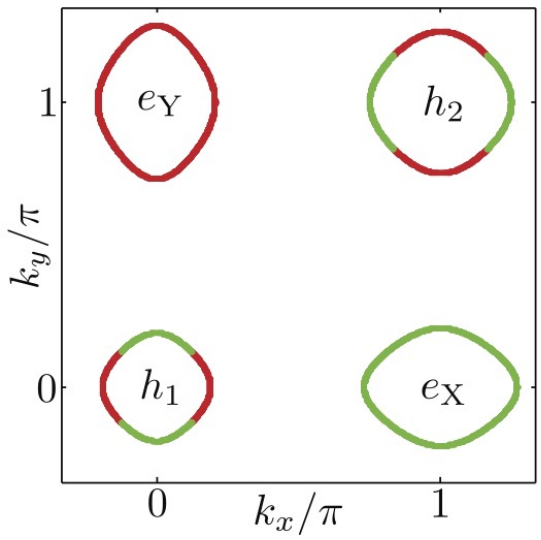

Figure 2.3: Fermi surface of the two-orbital model. Reproduced from Fernandes and Chubukov (2016)

Chapter 3

Variational Monte Carlo method

Quantum Monte Carlo methods are a family of computational algorithms whose aim is to provide reliable solutions for interacting quantum systems(Becca and Sorella (2017)). These methods work by constructing a stochastic sample of relevant configurations, which are selected according to a given probability distribution.

In the family of quantum Monte Carlo there is the Variational Monte Carlo (VMC), which allows us to obtain the physical properties of a given many-body state. The main advantage of VMC lies in the fact that it relies on the variational principle, i.e. the average value of the Hamiltonian over any wavefunction has a lower bound in the ground-state energy. VMC offers also some computational advantages like: the fact that it does not suffer from the sign problem and the fact that it is easily scalable to a large number of processors. The ground-state properties are obtained by optimizing the parameters of the Jastrow-Slater wavefunction through the stochastic reconfiguration method(Becca and Sorella (2017)). Another advantage of VMC is also the fact that it can treat more general Hamiltonians, i.e. models with long range interactions or different atomic orbitals, without a dramatic increase in computational cost, unlike other computational methods such as density-matrix renormalization group or tensor network methods (Becca and Sorella (2017)). Once the initial many-body state is chosen, its modulus squared is taken as the probability distribution for the algorithm. Of course VMC is not perfect, indeed it suffers from a bias due to the choice of the initial state, which may miss the correct properties of the ground state.

In this chapter we present first the formulation of the VMC approach and conclude by describing the Jastrow-Slater wavefunction.

3.1 Variational principle

Let $|\gamma_0\rangle$ (with energy E_0) be the exact ground state of a given Hamiltonian $\mathcal{H}$, then take $|\Psi_{var}\rangle$ as the approximate *ansatz* of $|\gamma_0\rangle$. We can define the variational energy of the state $|\Psi_{var}\rangle$ as:

$$E_{var} = \frac{\langle\Psi_{var}|\mathcal{H}|\Psi_{var}\rangle}{\langle\Psi_{var}|\Psi_{var}\rangle}. \tag{3.1}$$

As any state in the Hilbert space, $|\Psi_{var}\rangle$ can be expressed in terms of the eigenfunctions $|\gamma_i\rangle$ of $\mathcal{H}$:

$$\begin{aligned} |\Psi_{var}\rangle &= \sum_i a_i|\gamma_i\rangle \\ a_i &= \langle\gamma_i|\Psi_{var}\rangle. \end{aligned} \tag{3.2}$$

The normalization condition $\langle\Psi_{var}|\Psi_{var}\rangle = 1$ implies that $\sum_i |a_i|^2 = 1$.
If we calculate the energy difference between the variational and the ground state energy, we get

$$E_{var} - E_0 = \sum_{i\neq 0} |a_i|^2(E_i - E_0) \geq 0, \tag{3.3}$$

meaning that any initial variational state provides an upper bound of the exact energy; therefore all our efforts will be devoted to minimizing E_{var}. In order to do so we have to: consider all the states $|\Psi\rangle$ in the Hilbert space, calculate their average energy E and then, according to 3.3, take the lowest as E_0 and the corresponding state as the ground state. Such approach is unrealistic since in realistic scenarios the size of the Hilbert space grows exponentially with the system size. To solve this problem an *ansatz* is made regarding the wavefunction, i.e. we choose a functional form for $|\Psi_{var}\rangle$ that depends on a set of parameters to optimize. Making such an assumption is a gamble, indeed a wrong choice could lead to the impossibility of some behaviors showing up; for example, Hartree-Fock wavefuntions cannot describe a superconducting phase, a BCS wavefunction is necessary (Becca and Sorella (2017)).
It would seem that our problem is solved. What we have to do is simply comparing the variational energies of different wavefunctions and take the lowest value as the best approximation of E_0. However the analytical evaluation of the variational energy is usually impossible, therefore a numerical technique is needed. To do so Markov chains and the Metropolis algorithm come of help.
Now we describe the framework in which VMC methods are defined. We start by defining a many-body basis $|x\rangle$ in the Hilbert space, in which the states are orthogonal and normalized for simplicity, i.e. $\sum_x |x\rangle\langle x| = \mathbb{I}$. By plugging this completeness relation in 3.1 we get:

$$E_{var} = \frac{\sum_x \langle\Psi|x\rangle\langle x|\mathcal{H}|\Psi\rangle}{\sum_x \langle\Psi|x\rangle\langle x|\Psi\rangle} = \frac{\sum_x |\langle\Psi|x\rangle|^2 \frac{\langle x|\mathcal{H}|\Psi\rangle}{\langle x|\Psi\rangle}}{\sum_x |\langle\Psi|x\rangle|^2} = \sum_x \mathcal{P}(x)e_L(x), \tag{3.4}$$

where we defined the local energy (local estimator of $\mathcal{H}$ to be precise):

$$e_L(x) = \frac{\langle x|\mathcal{H}|\Psi\rangle}{\langle x|\Psi\rangle}, \tag{3.5}$$

while

$$\mathcal{P}(x) = \frac{|\langle\Psi|x\rangle|^2}{\sum_x |\langle\Psi|x\rangle|^2} \tag{3.6}$$

can be interpreted as a probability due to the fact that it is non negative and that $\sum_x \mathcal{P}(x) = 1$. This means that if we are able to generate a sequence of N configurations $|x_n\rangle$, that after thermalization are distributed according to $\mathcal{P}(x)$ (for example by using the Metropolis algorithm described below), we can calculate the value of E_{var} as:

$$E_{var} \approx \frac{1}{N}\sum_{n=1}^{N} e_L(x). \tag{3.7}$$

3.1.1 Zero-variance property

Let us suppose that the variational state $|\Psi\rangle$ we chose coincides with an eigenstate of $\mathcal{H}$. From the Schrödinger equation we get $\mathcal{H}|\Psi\rangle = E|\Psi\rangle$. If we use this fact inside the local energy formula we find:

$$e_L(x) = \frac{\langle x|\mathcal{H}|\Psi\rangle}{\langle x|\Psi\rangle} = E\frac{\langle x|\Psi\rangle}{\langle x|\Psi\rangle} = E, \tag{3.8}$$

implying that $e_L(x)$ does not depend on $|x\rangle$, meaning that the local energy has zero variance. This fact is very important because it shows the reduction of the statistical fluctuations while the minimization gradually reaches a stationary value.

3.2 Markov chains

A Markov chain is a stochastic process describing a sequence of configurations in which the probability of configuration x at time t_c, $p(x, t_c)$, depends only on the configuration of the system at the previous time instant t_{c-1} (in this case we assumed a unitary time step). Markov chains are useful because they allow us to build a particular sequence whose probability distribution converges to a desired one, meaning that we can use them to build a sequence converging to $\mathcal{P}(x)$ (3.6).
Using the fact that each configuration depends only on the previous one we can define a transition probability $q(x', x)$ (assumed to be time independent for simplicity) regulating the transition from state x to state x'. Being a probability, the following condition is met:

$$\sum_{x'} q(x', x) = 1. \tag{3.9}$$

If we consider the case of a finite space of configuration and finite time, the probability of being in state x' at time t_{c+1} is given by the Master equation of the chain

$$p(x', t_{c+1}) = p(x', t_c) + \sum_x [p(x, t_c)q(x', x) - p(x', t_c)q(x, x')]. \tag{3.10}$$

In order to reach a steady evolution, where the distribution converges to the desired one ($\mathcal{P}(x)$) it is sufficient that $\sum_x [p(x, t_c)q(x', x) - p(x', t_c)q(x, x')] = 0$, which is called global balance condition.

Usually a stronger condition which is enforced, named detailed balance:

$$\mathcal{P}(x)q(x',x) = \mathcal{P}(x')q(x,x'), \tag{3.11}$$

stating that there is no net flux of probability between states x and x'. To have the certainty that our Markov chain reaches a unique equilibrium distribution it is also necessary to require the process to be ergodic. A stochastic process is ergodic if any configuration can be reached by all the others in a finite number of steps.

However there is a problem in all this discussion, indeed the system's distribution stabilizes on the stationary one, $\mathcal{P}(x)$, in an infinite time. Of course our algorithm cannot run indefinitely, so we can make the approximation that the configurations are distributed according to $\mathcal{P}(x)$ after a large, but finite, time, the thermalization time t_{th}. Therefore we will compute the averages of observables using only the steps after t_{th}. Of course the problem is not actually solved because the question now is: "How do we determine the correct t_{th}?". There is no absolute answer. We simply check the iterations of the process and stop after the fluctuations are below a threshold established at the beginning.

3.3 Metropolis-Hastings algorithm

In this section, we present a way of constructing a probability distribution $q(x',x)$ that satisfies the detailed balance condition 3.11, such that the configuration distribution converges to $\mathcal{P}(x)$ in a finite number of steps. This procedure was first introduced by Metropolis and his collaborators (Metropolis et al. (1953)) and then was generalized by extending it to more general systems by Hastings (Hastings (1970)); therefore it goes by the name of Metropolis-Hastings algorithm.

As a first step we split the probability $q(x',x)$ in trial probability $T(x',x)$ and acceptance probability $A(x',x)$ obtaining:

$$q(x',x) = T(x',x)A(x',x). \tag{3.12}$$

The trial probability $T(x',x)$ can be chosen freely as long as ergodicity in ensured. The algorithm works by proposing a trial configuration x' which is accepted as the new configuration with probability $A(x',x)$. The acceptance probability is given by:

$$A(x',x) = \min\left[1, \frac{\mathcal{P}(x')T(x,x')}{\mathcal{P}(x)T(x',x)}\right]. \tag{3.13}$$

The proof that this acceptance probability satisfies the detailed balance is straightforward. Let us consider the case in which $\mathcal{P}(x')T(x,x')/\mathcal{P}(x)T(x',x) < 1$, then:

$$\begin{aligned} A(x',x) &= \frac{\mathcal{P}(x')T(x,x')}{\mathcal{P}(x)T(x',x)} \\ A(x,x') &= 1. \end{aligned} \tag{3.14}$$

Substituting these probabilities in 3.11 we get:

$$\mathcal{P}(x)T(x',x)\frac{\mathcal{P}(x')T(x,x')}{\mathcal{P}(x)T(x',x)} = \mathcal{P}(x')T(x,x'); \tag{3.15}$$

simplifying we find an identity proving that detailed balance is satisfied. In the same way we can prove this also for $\mathcal{P}(x')T(x,x')/\mathcal{P}(x)T(x',x) > 1$.
There is a simplified case of the algorithm: the case in which the trial probability is symmetric, i.e. $T(x',x) = T(x,x')$. In this case the acceptance probability is reduced to

$$A(x',x) = \min\left[1, \frac{\mathcal{P}(x')}{\mathcal{P}(x)}\right]. \tag{3.16}$$

As we can see in equation 3.13, or better in equation 3.16, it is important to know the equilibrium distribution $\mathcal{P}(x)$ up to a constant, since only the ratio between $\mathcal{P}(x)$ and $\mathcal{P}(x')$ is relevant. Another advantage is also the fact that if the configuration x' is near the previous configuration x all moves have a high probability to be accepted, since the ratio between $\mathcal{P}(x)$ and $\mathcal{P}(x')$ is almost 1.

3.3.1 Example: VMC for the Hubbard model

In this case the ratio of equilibrium probabilities is given by equation 3.6

$$\frac{\mathcal{P}(x')}{\mathcal{P}(x)} = \frac{|\langle\Psi|x'\rangle|^2}{|\langle\Psi|x\rangle|^2}, \tag{3.17}$$

where the normalization constant $\sum_x |\langle\Psi|x\rangle|^2$ is simplified.
State x is simply the many-electron configuration. In this case the Metropolis-Hastings algorithm is given by the following steps:

1. Generate random numbers i, j to select two sites from which we define the trial probability;
2. If an electron can hop from i to j, compute the acceptance probability $A(x',x)$, otherwise go back to 1);
3. Generate a number η from a uniform distribution $(0,1]$;
4. If $A(x',x) \geq \eta$ the new configuration x' is accepted, otherwise it is rejected;
5. Every N steps (where N is the number of electrons of the system) compute the observable for the configuration x';
6. Go to 1)

As observable we can take the local energy, or other functions such as energy squared.
After a sufficiently long thermalization time, the configurations are assumed to be distributed according to $\mathcal{P}(x)$ and we reach the set of equilibrium configurations $(x_1, \ldots, x_N)$. Using the local energies computed in the equilibrium configuration we can calculate the variational energy as:

$$E_{var} = \lim_{N\to\infty} \frac{1}{N} \sum_{i=1}^{N} e_L(x_i), \tag{3.18}$$

where $e_L(x_i)$ are the local energies.
Of course from a practical point of view taking the limit is impossible; therefore the resulting

variational energy will be affected by an error. We can calculate the errorbar as:

$$\Delta = \sqrt{\frac{1}{N(N-1)} \sum_{i=1}^{N} (\omega_N - \epsilon_N^2)}, \tag{3.19}$$

where

$$\begin{aligned} \omega_N &= \frac{1}{N} \sum_{i=1}^{N} e_L^2(x_i) \\ \epsilon_N &= \frac{1}{N} \sum_{i=1}^{N} e_L(x_i). \end{aligned} \tag{3.20}$$

The previous calculations for E_{var} and Δ are valid for an uncorrelated sample of the local energies $e_L(x_i)$. However samples produced by the Metropolis algorithm, described above, are affected by correlation, since each configuration is generated by the previous one. This phenomenon is emphasized when the acceptance ratio is small. To decrease correlation between samples a commonly used technique is the binning technique. This approach consists of taking a subsequence of measurements of length L_{bin} and block them together to compute the partial average energy:

$$E_j = \frac{1}{L_{bin}} \sum_{i=(j-1)L_{bin}+1}^{jL_{bin}} e_L(x_i), \tag{3.21}$$

where $j = 1, \ldots, N_{bin}$ and $N_{bin} = N/L_{bin}$. After the equilibration of the Markov chain the correlation function:

$$C(n-m) = \langle x_n x_m \rangle - \langle x_n \rangle \langle x_m \rangle \tag{3.22}$$

depends only on the time difference $n-m$ and goes to zero exponentially i.e. $C(n-m) \propto e^{-\frac{|n-m|}{\tau}}$ (τ is the correlation time in units of discrete time step). If L_{bin} is sufficiently larger than τ the bin averages can be considered to be independent random variables (Becca and Sorella (2017)). Therefore the variational energy remains the same because it is a linear function and can be computed as:

$$E_{var} = \frac{1}{N_{bin}} \sum_{j=1}^{N_{bin}} E_j, \tag{3.23}$$

and the errorbar can be calculated as:

$$\Delta = \sqrt{\frac{1}{N_{bin}(N_{bin}-1)} \sum_{j=1}^{N_{bin}} (E_j - E_{var})^2} \tag{3.24}$$

3.4 Stochastic reconfiguration method

VMC methods are aimed at minimizing the energy. To do so in this work we will use the stochastic reconfiguration algorithm (Sorella (1998), Sorella (2001), and Becca and Sorella (2017)).
Before starting the discussion let us first describe how to compute the derivatives of the variational energy with respect to a variational parameter α_k:

$$\frac{\partial E_\alpha}{\partial \alpha_k} = \frac{\partial}{\partial \alpha_k} \frac{\langle \Psi_\alpha | \mathcal{H} | \Psi_\alpha \rangle}{\langle \Psi_\alpha | \Psi_\alpha \rangle}. \tag{3.25}$$

To differentiate the variational energy we expand the state α_k for a small change $\alpha_k \to \alpha_k + \delta\alpha_k$. Taking a wavefunction $\Psi_\alpha(x)$, from a configuration $|x\rangle$, we can write its change as:

$$\Psi_{\alpha+\delta\alpha_k}(x) = \Psi_\alpha(x) + \delta\alpha_k \frac{\partial \Psi_\alpha(x)}{\partial \alpha_k} + O(\delta\alpha_k^2), \tag{3.26}$$

where $\alpha + \delta\alpha_k$ means that we shift the k-th component of the vector α of $\delta\alpha_k$. We now define the local operator $\mathcal{O}_k$ such that:

$$\begin{aligned} \langle x|\mathcal{O}_k|x'\rangle &= \delta_{x,x'}\mathcal{O}_\alpha(x) \\ \mathcal{O}_\alpha(x) &= \frac{\partial \ln \Psi_\alpha(x)}{\partial \alpha_k} = \frac{1}{\Psi_\alpha(x)}\frac{\partial \Psi_\alpha(x)}{\partial \alpha_k}. \end{aligned} \tag{3.27}$$

Using the local operator we can write an equation for the evolution of $|\Psi_\alpha\rangle$:

$$|\Psi_{\alpha+\delta\alpha_k}\rangle = (1 + \delta\alpha_k \mathcal{O}_k)|\Psi_\alpha\rangle. \tag{3.28}$$

Using the local operator we can also rewrite equation 3.25 as:

$$\frac{\partial E_\alpha}{\partial \alpha_k} = \frac{\langle\Psi_0|(\mathcal{O}_k\mathcal{H} + \mathcal{H}\mathcal{O}_k)|\Psi_0\rangle}{\langle\Psi_0|\Psi_0\rangle} - 2\frac{\langle\Psi_0|\mathcal{O}_k|\Psi_0\rangle\langle\Psi_0|\mathcal{H} + \mathcal{H}\mathcal{O}_k|\Psi_0\rangle}{\langle\Psi_0|\Psi_0\rangle^2}. \tag{3.29}$$

We begin with the Jastrov-Slater wavefunction, to be defined later in section 3.5, $|\Psi_0\rangle \equiv |\Psi(\alpha_k^0)\rangle$ depending on the variational parameters α_k^0, where $k = 1, \ldots, p$. The energy is then varied by a constant shift yielding the a new state $|\Psi_\Lambda\rangle$ such that

$$|\Psi_\Lambda\rangle = (\Lambda - \mathcal{H})|\Psi_0\rangle. \tag{3.30}$$

The new wavefunction will unlikely be in Jastrow-Slater form, hence we have to approximate it with the closest quantum state $|\Psi(\alpha_k')\rangle$ (for simplicity we will name it $|\Psi'\rangle$), that we always take in Jastrow-Slater form. To make such approximation we consider a small variation $\delta\alpha$ in the variational parameters vector α:

$$\alpha' = \alpha + \delta\alpha. \tag{3.31}$$

This variation induces a change in $|\Psi_0\rangle$ which can be expressed with a first order Taylor expansion in $\delta\alpha$:

$$|\Psi'\rangle = \delta\alpha_0|\Psi_0\rangle + \sum_{k=1}^{p} \delta\alpha_k \frac{\partial|\Psi_0\rangle}{\partial\alpha_k} + O(\delta\alpha_k^2). \tag{3.32}$$

Here $\delta\alpha_k$ are the components of $\delta\alpha$ and $\delta\alpha_0$ is a parameter inserted just to match the normalization condition. We can rewrite this expansion using local operators as:

$$|\Psi'\rangle = \sum_{k=0}^{p} \delta\alpha_k \mathcal{O}_k|\Psi\rangle. \tag{3.33}$$

In the stochastic reconfiguration method we impose that the projections of $|\Psi_\Lambda\rangle$ and $|\Psi'\rangle$ into the subspace defined by $\mathcal{O}_i|\Psi_0\rangle$ are equal, namely

$$\langle\Psi_0|\mathcal{O}_i|\Psi'\rangle = \langle\Psi_0|\mathcal{O}_i|\Psi_\Lambda\rangle, \tag{3.34}$$

ensuring that the energy computed from $|\Psi'\rangle$ is lower than the energy computed from $|\Psi_0\rangle$. Substituting 3.30 and 3.33 in 3.34 we get:

$$\begin{aligned} \sum_{k=0}^{p} \delta\alpha_k \langle \mathcal{O}_i \mathcal{O}_k \rangle &= \langle \mathcal{O}_i (\Lambda - \mathcal{H}) \rangle \\ \langle \dots \rangle &= \langle \Psi_0 | \dots | \Psi_0 \rangle. \end{aligned} \tag{3.35}$$

For $j = 0$, by imposing that $\mathcal{O}_i \equiv \mathbb{I}$, equation 3.35 reads:

$$\delta\alpha_0 + \sum_{k=1}^{p} \delta\alpha_k \langle \mathcal{O}_k \rangle = \Lambda - \langle \mathcal{H} \rangle, \tag{3.36}$$

since α_0 is involved only in the normalization we can solve for $\delta\alpha_0$:

$$\delta\alpha_0 = \Lambda - \langle \mathcal{H} \rangle - \sum_{k=1}^{p} \delta\alpha_k \langle \mathcal{O}_k \rangle. \tag{3.37}$$

Instead for $j \neq 0$ we get:

$$\delta\alpha_0 \langle \mathcal{O}_i \rangle + \sum_{k=1}^{p} \delta\alpha_k \langle \mathcal{O}_i \mathcal{O}_k \rangle = \Lambda \langle \mathcal{O}_i \rangle - \langle \mathcal{O}_i \mathcal{H} \rangle, \tag{3.38}$$

then by substituting 3.37 in 3.38

$$\sum_{k=1}^{p} \delta\alpha_k (\langle \mathcal{O}_i \mathcal{O}_k \rangle - \langle \mathcal{O}_i \rangle \langle \mathcal{O}_k \rangle) = \langle \mathcal{O}_i \rangle \langle \mathcal{H} \rangle - \langle \mathcal{O}_i \mathcal{H} \rangle. \tag{3.39}$$

Now we define a $p \times p$ matrix S, named covariance matrix, whose S_{ik} element is

$$S_{ik} = \langle \mathcal{O}_i \mathcal{O}_k \rangle - \langle \mathcal{O}_i \rangle \langle \mathcal{O}_k \rangle; \tag{3.40}$$

such matrix is symmetric and semi positive-definite. We also define a vector $\mathbf{f}$, containing the generalized forces, whose components are given by:

$$f_i \equiv \langle \mathcal{O}_i \rangle \langle \mathcal{H} \rangle - \langle \mathcal{O}_i \mathcal{H} \rangle. \tag{3.41}$$

This terms are named generalized forces because they are actually the derivative of the energy with respect to parameters in α, indeed following from 3.29

$$\frac{\partial E_\alpha}{\partial \alpha_i} = -2 f_i. \tag{3.42}$$

From a practical point of view, what we do is performing a Monte Carlo simulation at fixed parameters to compute both the covariances and generalized forces, then we use them to compute the variations of the parameters, i.e.

$$\delta\alpha_k = \sum_{i=1}^{p} S_{ki}^{-1} f_i. \tag{3.43}$$

Using this set $\delta\alpha_k$ we update the variational parameters, i.e. $\alpha_k' = \tau \delta\alpha_k$. τ is a parameter that regulates the convergence speed. Indeed, the larger τ is, the faster is the convergence of the

algorithm. So it seems that we have to take it as large as possible by paying attention, however, at the fact that for a too large value the algorithm may become unstable. Indeed, a small enough value of τ keeps the energy from increasing at each iteration. This can be seen from the first order expansion of the energy in τ:

$$\begin{aligned} E(\Psi') &= E(\Psi_0) + \sum_k^p \frac{\partial E(\Psi_0)}{\partial \alpha_k} \delta\alpha_k + O(\tau^2) \\ &= E(\Psi_0) - \sum_{k,i}^p S_{ki}^{-1} f_i f_k + O(\tau^2). \end{aligned} \tag{3.44}$$

Since the covariance matrix S is semi positive-definite so is S^{-1}; therefore the sum will be non negative and $E(\Psi') \leq E(\Psi_0)$. This proves that the algorithm converges to an energy minimum, however such minimum may not be the absolute minimum but just a local one.

3.5 Jastrow-Slater wavefunctions

The choice of the initial wavefunction is crucial to obtain the correct physical behavior of the system, however it cannot be too complex otherwise calculations will take too long. In the case of correlated superconductors it is fundamental to describe the effect of the Hubbard U in reducing the weight of configurations in multiply-occupied states. To do so in 1963 Gutzwiller introduced a wavefunction starting from the non interacting ground state $|\Phi_0\rangle$

$$|\Psi_G\rangle = \mathcal{P}_G |\Phi_0\rangle. \tag{3.45}$$

Gutzwiller constructed the new wavefunction by applying an operator $\mathcal{P}_G$ with the effect of suppressing configurations with multiply occupied sites. The operator $\mathcal{P}_G$ is named Gutzwiller factor and depends only on a single parameter g ($g > 0$ for repulsive Hubbard U):

$$\mathcal{P}_G = \exp\left[-g \sum_i n_{i,\downarrow} n_{i,\uparrow}\right], \tag{3.46}$$

where n is the average density. If we take the basis with electrons localized on every site $|x\rangle$ and expand $|\Psi_G\rangle$ we obtain:

$$\mathcal{P}_G = \sum_x e^{-gN_d(x)} \langle x|\Phi_0\rangle |x\rangle, \tag{3.47}$$

where $N_d(x)$ is the number of doubly occupied sites in configuration $|x\rangle$. When $U = 0$ the ground state is obtained by imposing $g = 0$, while for the $U/t \to \infty$ limit also $g \to \infty$ yielding a state with no double-occupation. For finite value of g the state is in a metallic phase. The problem with this description is the fact that when doubly occupied states are created they are free to move inside the lattice independently giving rise to electrical conduction in presence of an external field (Capello et al. (2005)); they are fixed in place only in the $g \to \infty$ case.

In order to have a more accurate description of the insulator we have to consider all the spatial

correlations (Capello et al. (2005)), following the proposal by Jastrow:

$$|\Psi_J\rangle = \mathcal{J}|\Phi_0\rangle. \tag{3.48}$$

where

$$\mathcal{J} = \exp\left[-\frac{1}{2}\sum_{i,j} v_{i,j}(n_{i,\uparrow}+n_{i,\downarrow})(n_{j,\uparrow}+n_{j,\downarrow})\right]. \tag{3.49}$$

$v_{i,j}$ is a pseudo-potential for density-density correlations in the variational state. In case of translationally invariant models, like Hubbard model, the pseudo-potential depends only on the relative distance $|\mathbf{R}_i - \mathbf{R}_j|$. It is also interesting to notice that the case $i = j$ coincides with the Gutzwiller factor discussed above. The Jastrow factor can be easily generalized to a multi-orbital system:

$$\mathcal{J} = \exp\left[-\frac{1}{2}\sum_{i,j,\alpha,\beta} v_{i,j}^{\alpha,\beta}(n_{i,\alpha,\uparrow}+n_{i,\alpha,\downarrow})(n_{j,\beta,\uparrow}+n_{j,\beta,\downarrow})\right], \tag{3.50}$$

where α, β are orbital indices.

3.5.1 Jastrow-Slater wavefunction of the two-orbital Hubbard model

In this work we study a two-orbital model for iron-based superconductors. To do so we take a BCS uncorrelated state $|\Psi_0\rangle$ and then add the electron-electron correlations with the use of two Jastrow factors, i.e:

$$|\Psi\rangle = \mathcal{J}_C\mathcal{J}_S|\Psi_0\rangle. \tag{3.51}$$

The uncorrelated state $|\Psi_0\rangle$ is given by $\mathcal{H}_0$ (from eq.2.8) with the inclusion of a BCS intra-orbital pairing, i.e:

$$\mathcal{H}_{BCS} = \mathcal{H}_0 - \sum_{R,\alpha,\sigma}\mu_\alpha c^\dagger_{R,\alpha,\sigma}c_{R,\alpha,\sigma} + \sum_{R,\alpha,\delta}[\Delta_{\alpha,\delta}(c_{R,\alpha,\uparrow}c_{R+\delta,\alpha,\downarrow} - c_{R,\alpha,\downarrow}c_{R+\delta,\alpha,\uparrow} + h.c.)], \tag{3.52}$$

where $\delta \in (x, y, x+y, x-y)$ indicates nearest and next-nearest neighbors. R indicates a site in the lattice, while μ_α is the chemical potential of orbital α. $\Delta_{\alpha,\delta}$ and μ_α are optimized along the VMC run while the hoppings in $\mathcal{H}_0$ are kept constant. Electron-electron correlations are included by two Jastrow factors, one for long-range correlations and the other for Hund's coupling. Such factors have the form:

$$\begin{aligned}\mathcal{J}_C &= \exp\left[-\frac{1}{2}\sum_{i,j,\alpha,\beta} v_{i,j}^{\alpha,\beta}(n_{i,\alpha,\uparrow}+n_{i,\alpha,\downarrow})(n_{j,\beta,\uparrow}+n_{j,\beta,\downarrow})\right] \\ \mathcal{J}_S &= \exp\left[\sum_i u_i S^z_{i,xz}S^z_{i,yz}\right],\end{aligned} \tag{3.53}$$

where $n_{i,\alpha,\uparrow} + n_{i,\alpha,\downarrow}$ and $S^z_{i,\alpha} = (n_{i,\alpha,\uparrow} - n_{i,\alpha,\downarrow})/2$ are respectively the electron density and spin along the z axis on site i and orbital α. The parameters $v_{i,j}^{\alpha,\beta}$ and u_i are the pseudo-potentials to be optimized along the VMC run. The factor $\mathcal{J}_C$ is the charge density factor and encodes in the model the long range correlations, which are fundamental for Mott physics. The factor $\mathcal{J}_S$ is the spin factor and includes Hund's coupling, indeed, its effect is limited to spin-spin correlations on the same site.

Chapter 4

Results

In this chapter we investigate if the two-orbital model, whose Hamiltonian was discussed in section 2.3.2, may be complete enough to correctly describe the superconductive behavior of iron-based superconductors. We first study the Fermi surface in absence of correlations ($U = 0$), then we introduce the charge and spin Jastrow factors to investigate the effects of correlations and Hund's coupling (see Sec.3.5.1). The study has been carried out in different *doping* regimes: half filling, 10% hole/electron doping, 20% hole/electron doping. In the end, we investigate the emergence of superconductive correlations and how they relate to orbital selectivity. All reported simulations have been run both on a 6×6 and a 12×12 square lattice with two orbitals per site and periodic boundary conditions. In all simulations the tight-binding parameters are: $t_1 = -330$meV, $t_2 = 385$meV, $t_3 = -234$meV, $t_4 = -260$meV; also the ratio J/U has been fixed at 0.2 in all calculations.

4.1 Fermi surface of the tight-binding model at U=0

As we can see in figure 4.1 the Fermi surface presents two hole pockets (in red) and two electron pockets (in blue). The hole pockets are centered respectively at $(0, 0)$ and at (π, π), while the two electron pockets are centered at $(0, \pi)$ and $(\pi, 0)$. This is actually incorrect, since in the five-orbital model the two hole pockets are centered in $(0, 0)$ (Fernandes and Chubukov (2016)). However this discrepancy has been solved by considering the folded crystallographic cell, containing two Fe atoms, in which the two hole pockets are centered around $(0, 0)$ (Raghu et al. (2010)).

4.2 6×6 lattice

In this section we discuss the 6×6 lattice in the different regimes presented at the beginning of the chapter and focus on understanding how the BCS variational parameters $\Delta_{\alpha,\delta}$ behave especially out of half-filling. This is important since finite values of BCS parameters are a fundamental prerequisite for superconductivity, which will then be studied in a 12×12 lattice.

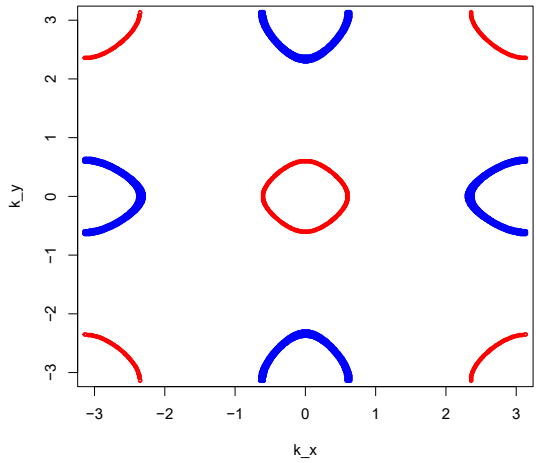

Figure 4.1: Fermi surface of the two-orbital tight-binding model. Hole pockets have been colored red, while electron pockets are blue

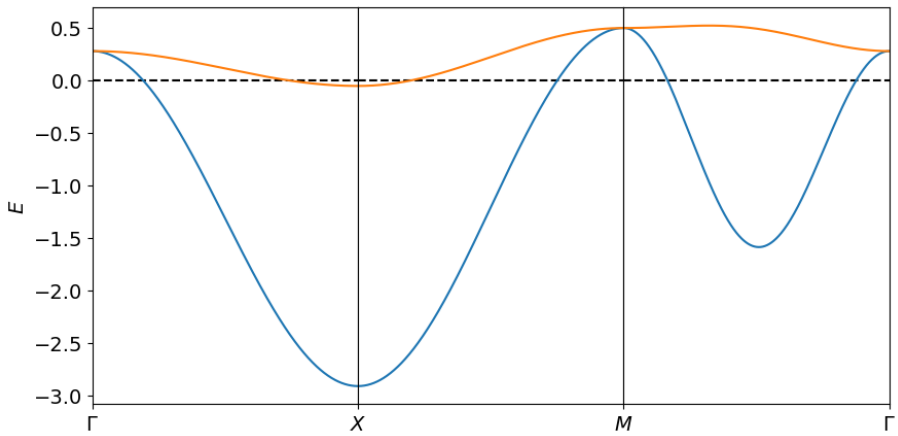

Figure 4.2: Plot of the band structure of the tight-binding model. There are two electron pockets (in blue), and two hole pockets (in orange)

4.2.1 Half-filling

We begin our analysis at half-filling. In this situation the system is expected to be a Mott-insulator at large values of U. We see that the optimal values of the BCS variational parameters are oscillating around zero for all values of U considered (see fig.4.3). From the point of view of orbital selectivity we see that the two orbitals have practically the same electronic occupation (see fig.4.4), where we defined the electronic occupation as $\frac{1}{L}\sum_R n_{R,\alpha}$, where $n_{R,\alpha} = n_{R,\alpha,\uparrow} + n_{R,\alpha,\downarrow}$ ($n_{R,\alpha,\sigma} = c^\dagger_{R,\alpha,\sigma} c_{R,\alpha,\sigma}$) and L is the number of sites in the lattice.

Our interest in orbital selectivity rises from the fact that, from calculations for the three-orbital model, it has been found that the appearance of superconductivity is strongly linked with orbital-selective correlations (Marino et al. (2024)).

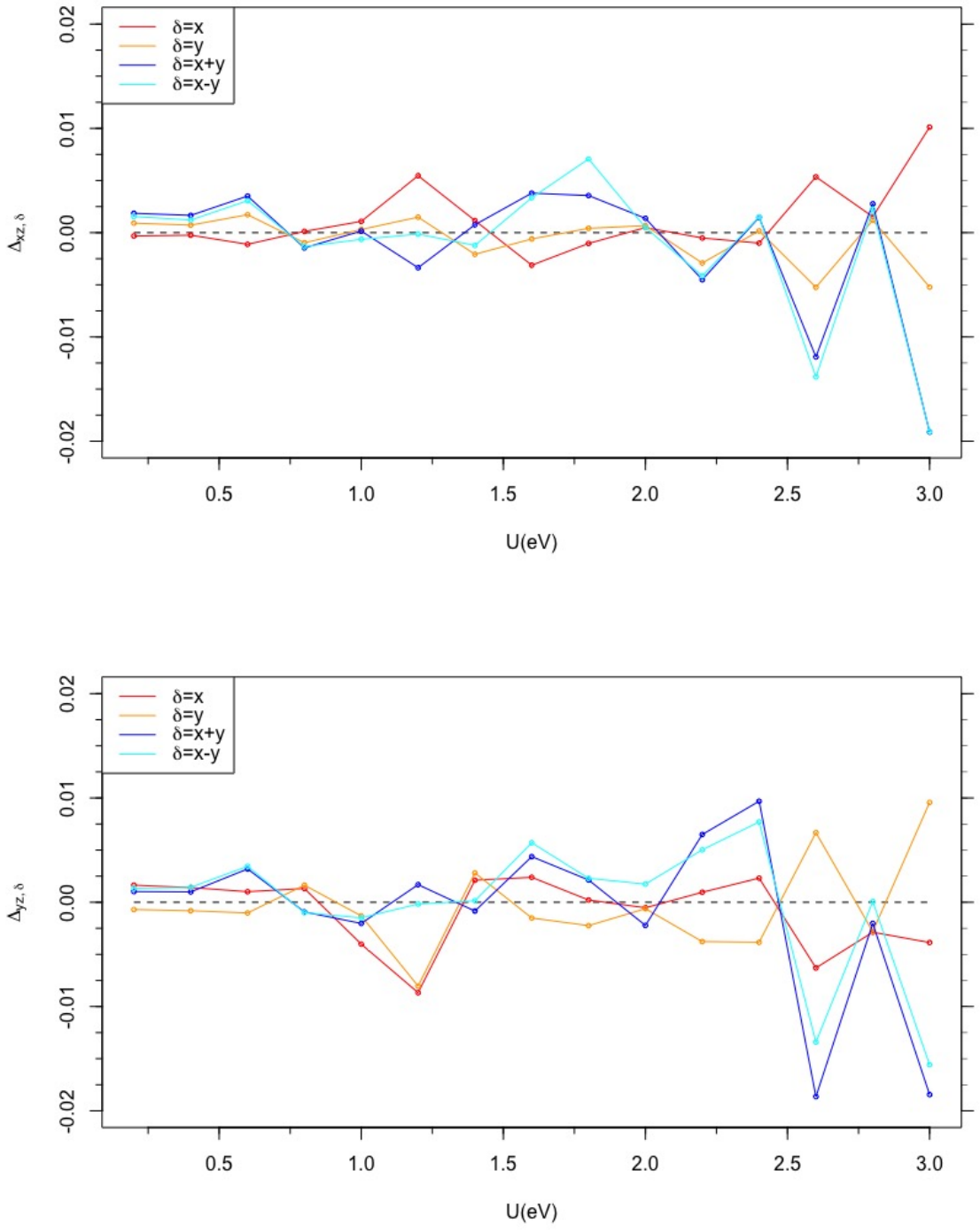

Figure 4.3: Optimal values of intra-orbital BCS parameters as function of U in the half-filling regime. Upper panel: optimal values for xz orbital. Lower panel: optimal values for yz orbital.

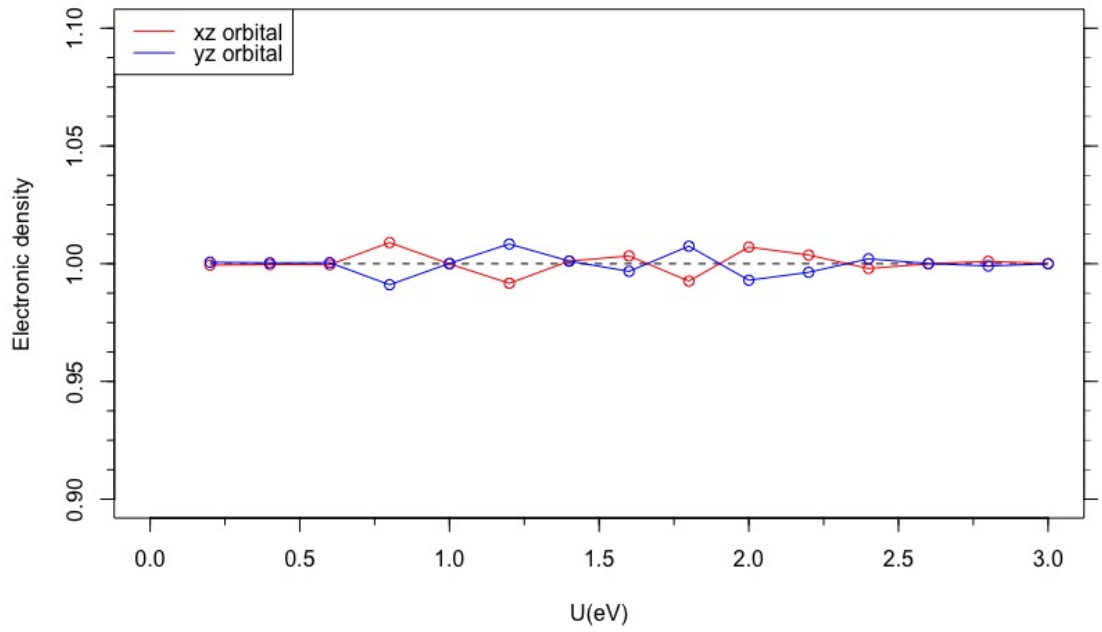

Figure 4.4: Electronic density per orbital, as a function of U, obtained in the half-filling regime

4.2.2 10% doping regime

We see that there is a notable difference between the two *doping* regimes. Indeed, the hole-doped regime features an orbital selective behavior, where orbital xz is clearly favored (see fig.4.5). This behavior is accompanied by the fact that there is a symmetry breaking with the effect that, for large values of U, the BCS parameters assume values different from zero with a definite symmetry, no longer oscillating around zero (see fig.4.7). In our case the parameter $\Delta_{xz,y}$ shows the greatest deviation from zero, making the xz orbital a candidate for significant pairing correlations, since in the three-orbital model such behavior leads to significant pairing correlations (Marino et al. (2024)). However, we cannot be certain of that, due to the fact that the lattice size is too small to get significant results in terms of superconductive correlations.

The electron doping regime instead shows a behavior similar to the half-filling regime (see fig.4.6). It is clear that there is no symmetry breaking and also that the occupations are fluctuating around the value 1.10, which is the value for which the two orbitals have the same occupation (see fig.4.5). However we can notice that the fluctuations are enhanced with respect to the half-filling regime (see fig.4.4).

What is interesting to see in this regime is the fact that it seems that orbital selectivity and superconductivity are strongly intertwined in IBS (Marino et al. (2024)), i.e. superconductivity cannot appear without orbital selectivity also in the two-orbital model.

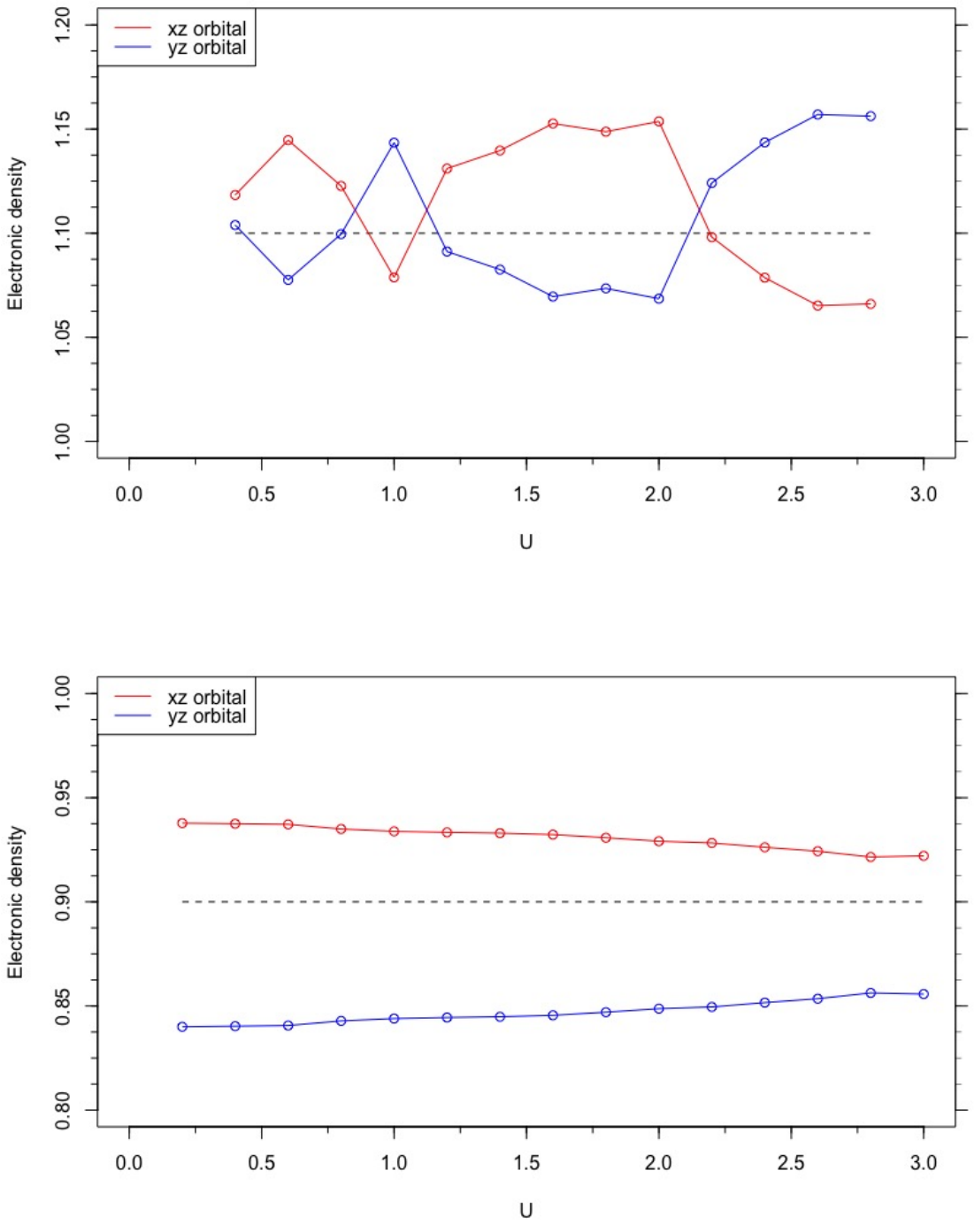

Figure 4.5: Upper panel: Electronic density of the two orbitals when the system is in 10% electron doping regime. Lower panel: Electronic density of the two orbitals when the system is in 10% hole doping regime.

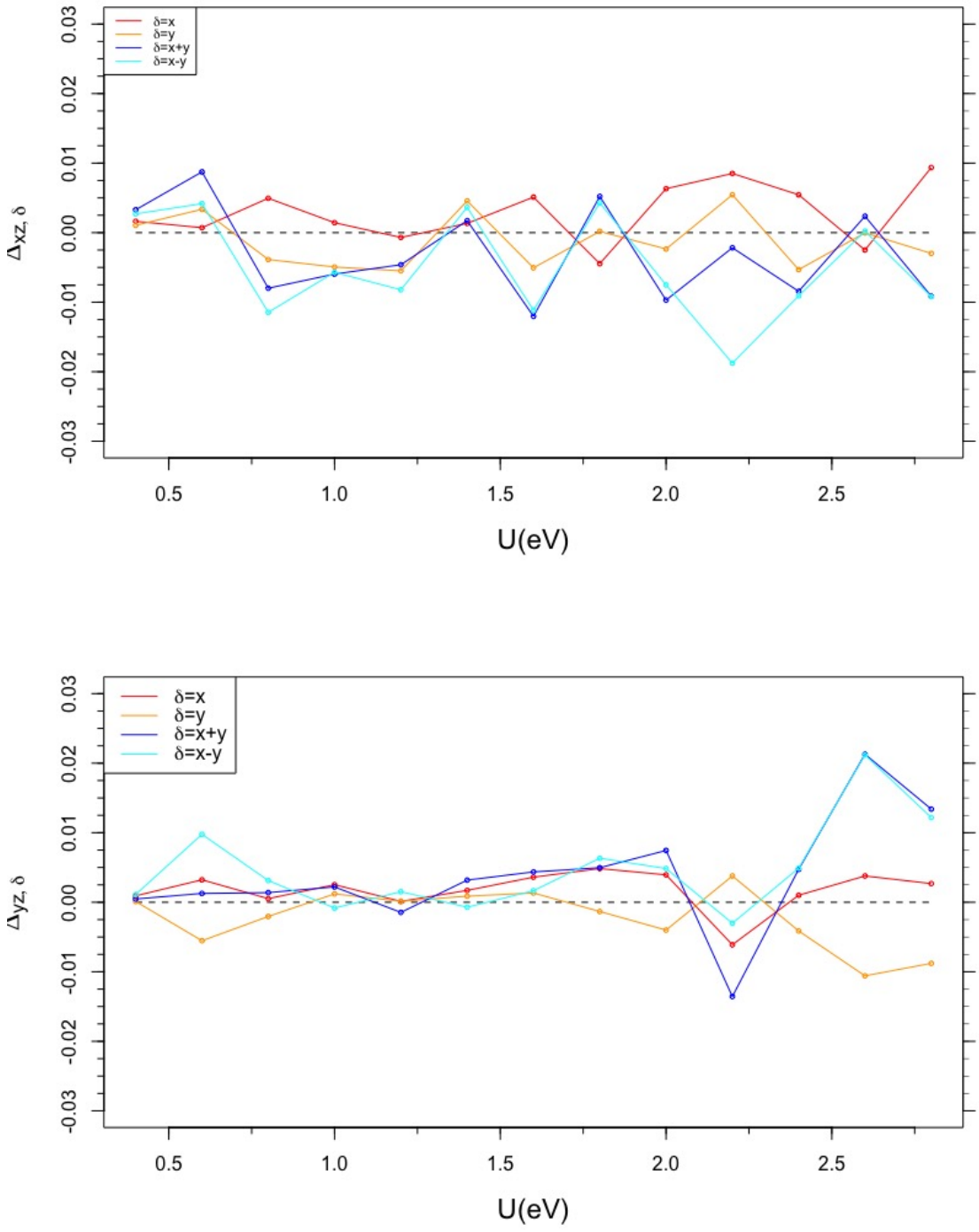

Figure 4.6: Upper panel: Optimal BCS parameters for orbital xz at 10% electron doping. Lower panel: Optimal BCS parameters for orbital yz at 10% electron doping

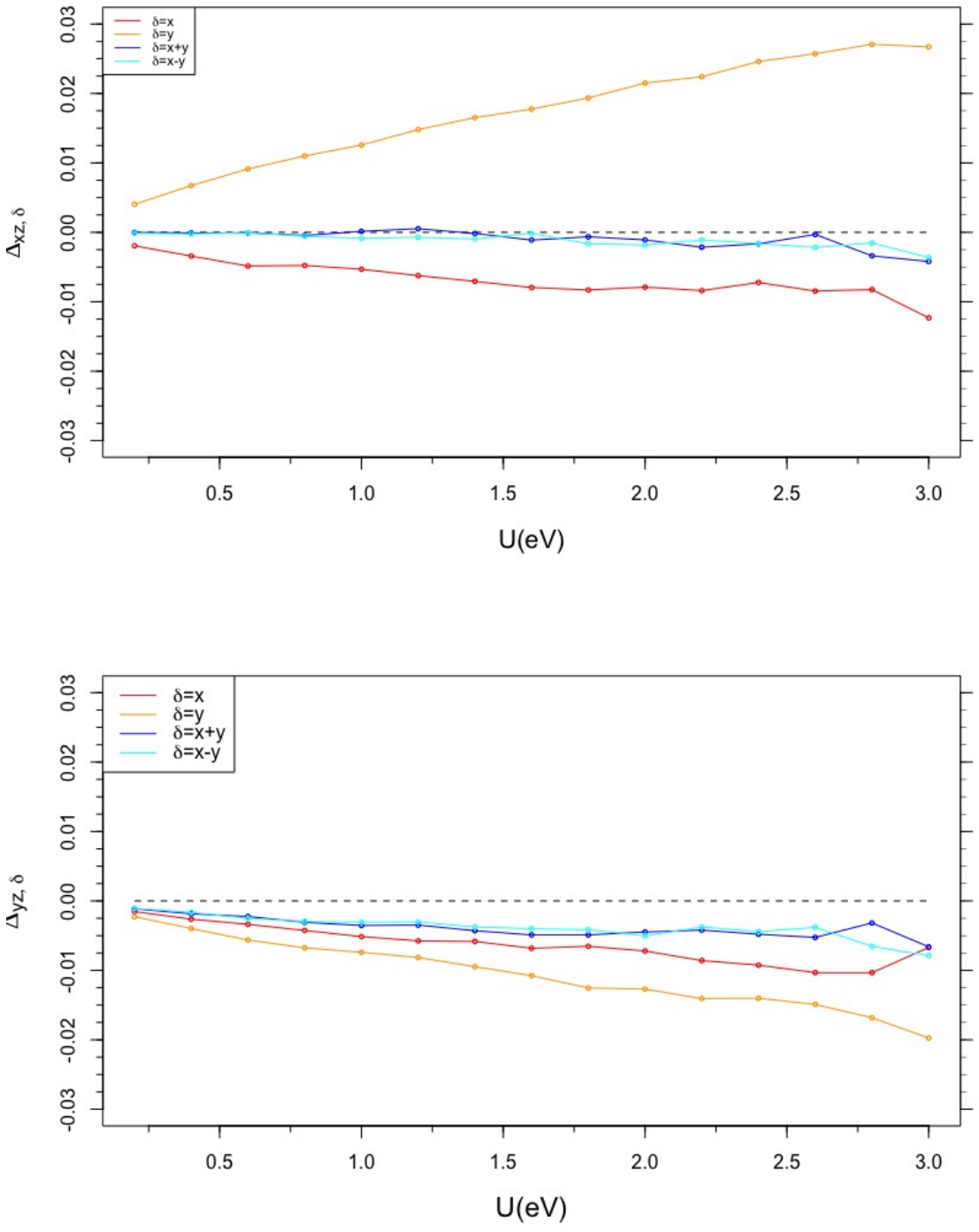

Figure 4.7: Upper panel: Optimal BCS parameters for orbital xz at 10% hole doping. Lower panel: Optimal BCS parameters for orbital yz at 10% hole doping

4.2.3 20% doping regime

As we can see from figure 4.8, increasing the *doping* did not change much in the case of electron-*doping* regime in terms of orbital selectivity, indeed the system does not privilege any of the two orbitals. What can be observed is the fact that for increasing values of U the system tends to stabilize the occupation of each orbital at the same value. Regarding the BCS parameters, we see in figure 4.9 that they oscillate around zero for increasing values of U, for both xz and yz orbitals corroborating the fact that there is no orbital selectivity.

The hole-*doping* regime behavior is much different from the 10% *doping* case. As we can see in figure 4.8 the xz orbital is no longer favored by the system, instead both electronic densities fluctuate around the same value. Since there is no orbital selectivity, we can expect the BCS parameters to fluctuate around zero. Indeed, as we can see in figure 4.10 there is no longer that symmetry characterizing the 10% *doping* regime (see figure 4.7).

Based on results obtained in this regime and the previous one (see section 4.2.2), we can start making an hypothesis, to be verified later in larger lattices, on the link between superconductivity and orbital selectivity, i.e. that in IBS without orbital selectivity there is no superconductivity.

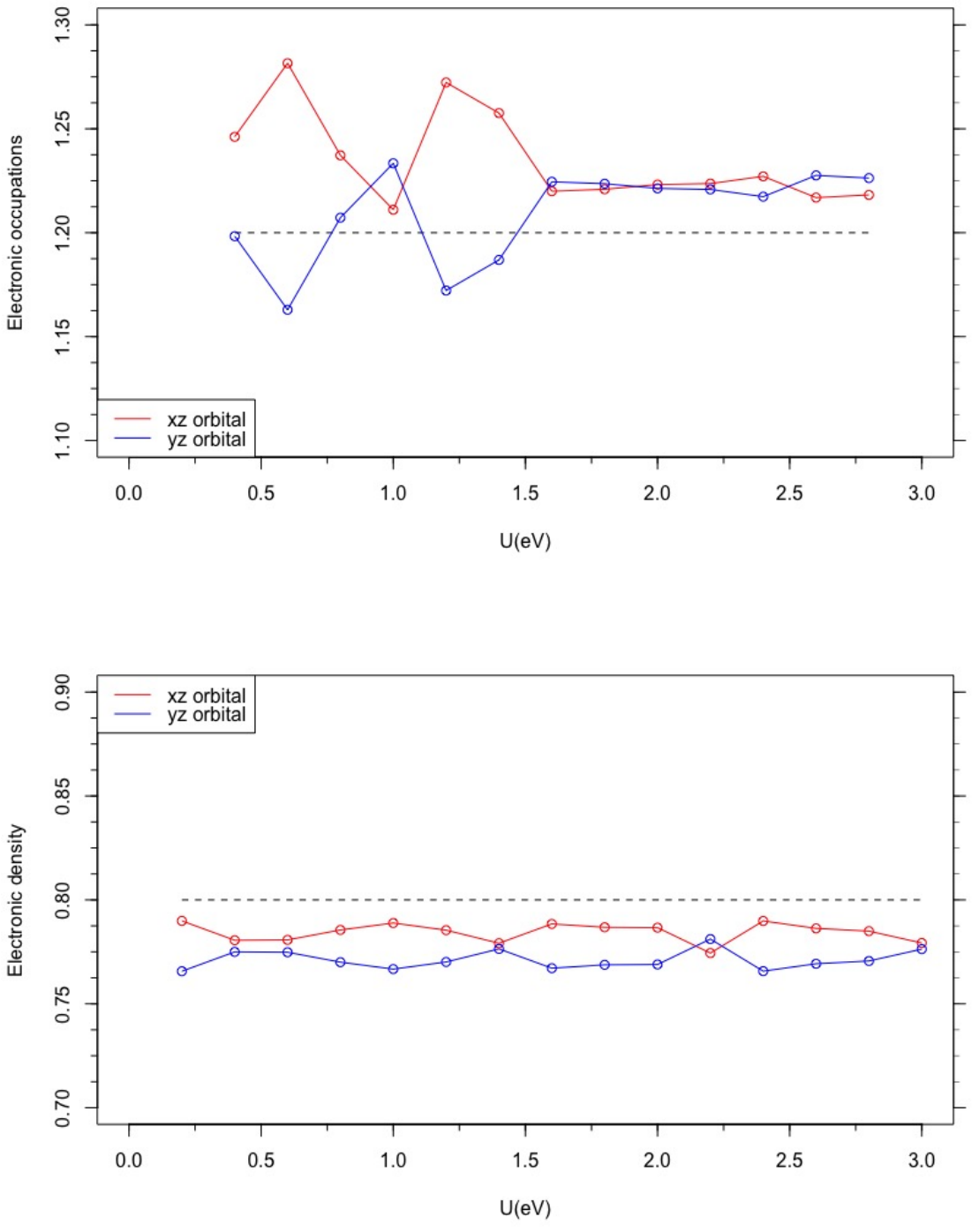

Figure 4.8: Upper panel: Electronic density of the two orbitals when the system is in 20% electron doping regime. Lower panel: Electronic density of the two orbitals when the system is in 20% hole doping regime.

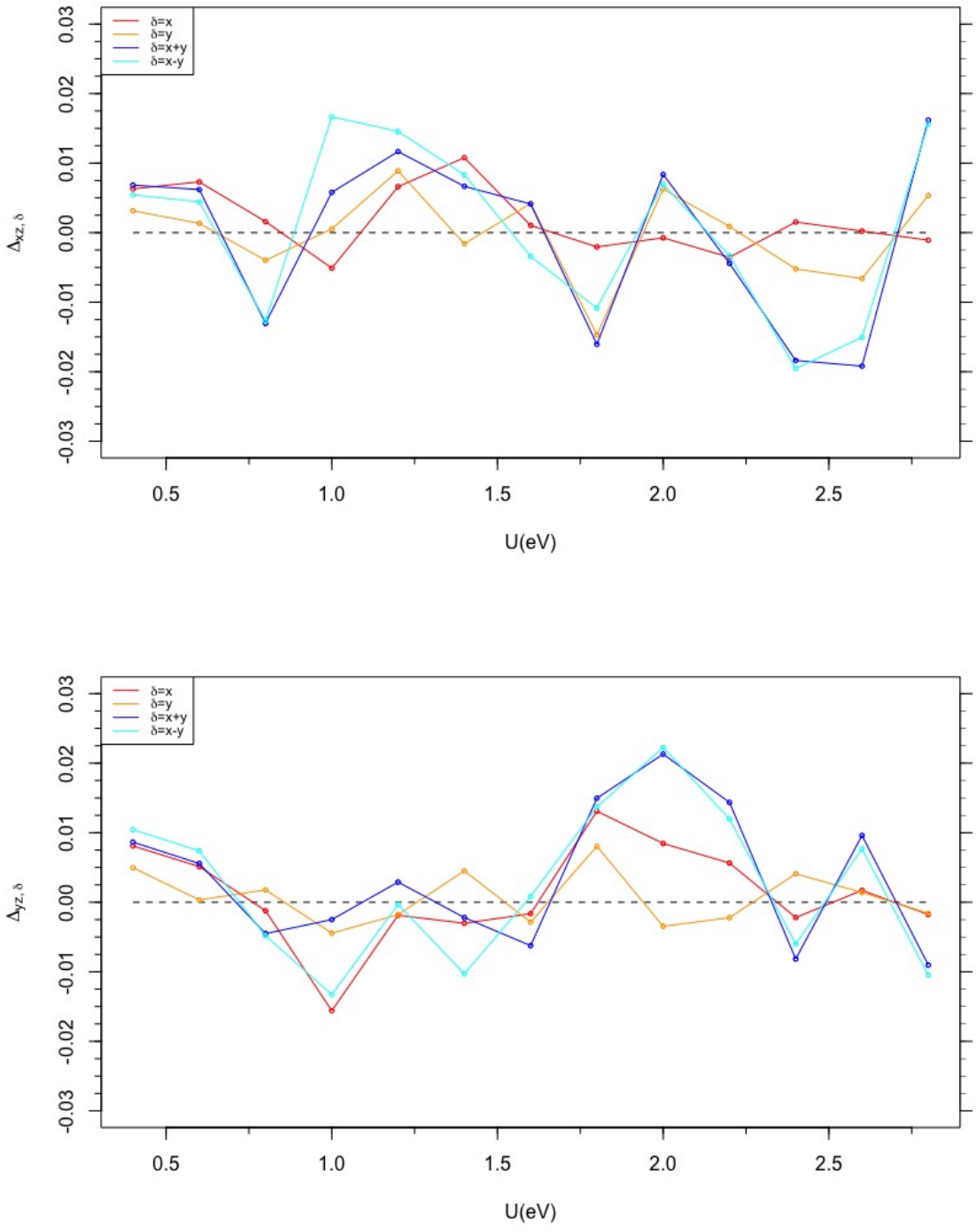

Figure 4.9: Upper panel: Optimal BCS parameters for orbital xz at 20% electron doping. Lower panel: Optimal BCS parameters for orbital yz at 20% electron doping

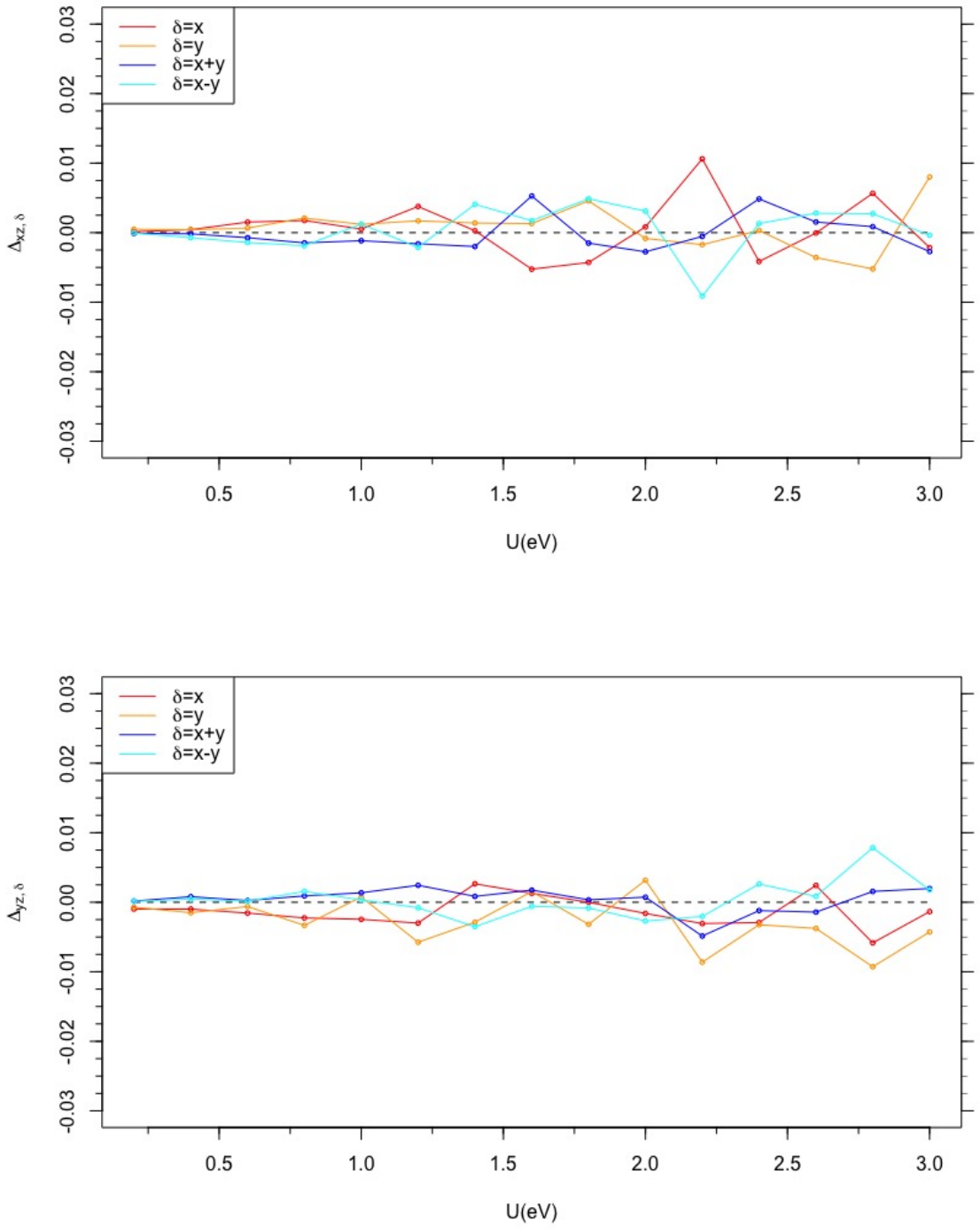

Figure 4.10: Upper panel: Optimal BCS parameters for orbital xz at 20% hole doping. Lower panel: Optimal BCS parameters for orbital yz at 20% hole doping

4.3 12×12 lattice

We now move to verify if the hypothesis, no orbital selectivity equals no superconductivity, is correct. To do so we have to compute superconductive correlations. In principle, they could be computed from $\mathcal{H}_{BCS}$ (see equation 3.52) since the pairing of electrons is included in the uncorrelated state, however the Jastrow factor (see equation 3.53) may suppress those pairing correlations. For instance, this is true in the Mott regime (Capello et al. (2005)). Therefore, we resort to computing intra-orbital pairing correlations, given by:

$$\mathcal{D}_\alpha(r) = \frac{1}{L}\sum_R \langle P_{R,\alpha} P^\dagger_{R+rx,\alpha}\rangle, \tag{4.1}$$

where L is the lattice size, and $P_{R,\alpha} = c_{R+y,\alpha,\downarrow}c_{R,\alpha,\uparrow} - c_{R+y,\alpha,\uparrow}c_{R,\alpha,\downarrow}$ is an operator that destroys two electrons on the same orbital at nearest neighbors along y. The idea is to study the correlation between a pair, made of two neighboring electrons along y, in position r, moving along x, and the same pair at the initial position. The system is superconductive if $\lim_{r\to\infty}\mathcal{D}_\alpha(r)$ remains finite. Of course it is impossible to consider an infinitely long lattice, hence we run our calculations on a lattice large enough to show if $\mathcal{D}_\alpha(r)$ goes to zero or stays finite. Therefore calculations could not have been made in the 6×6 lattice since the pair cannot make enough steps .

4.3.1 Half-filling

Again we begin our discussion with the half-filling regime. The system is expected to be a Mott insulator at large values of U and should not show orbital selectivity. As we can see in figure 4.11 some of the BCS parameters of orbital xz are significantly different from zero at high values of U, however the orbital cannot become superconductive since we are at half-filling and correlations are suppressed by the Jastrow factor(Capello et al. (2005)); instead, BCS parameters of orbital yz keep oscillating around zero. It is evident from figure 4.12 that for increasing values of U the two orbitals tend to have the same occupation.

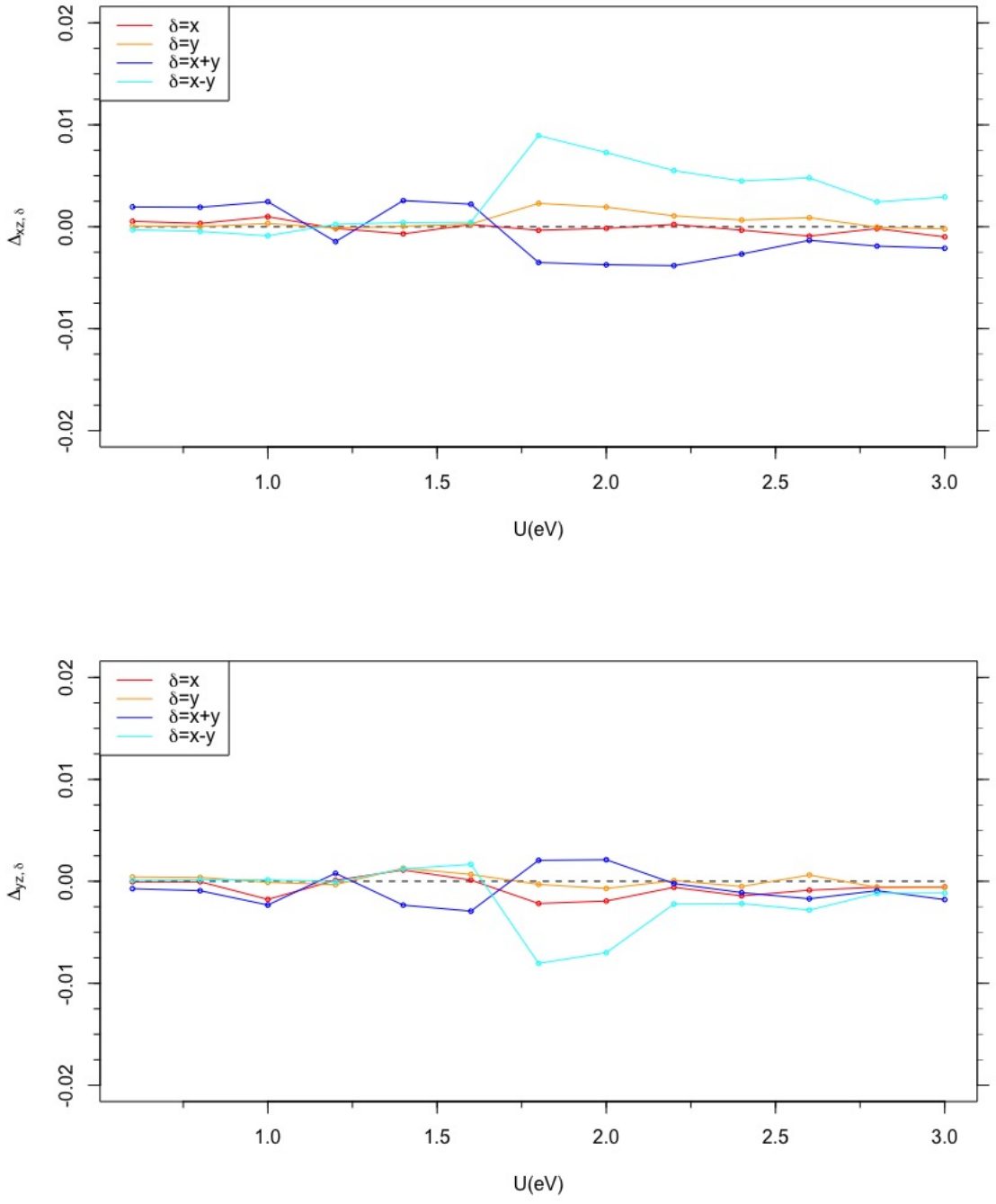

Figure 4.11: Upper panel: Optimal BCS parameters for orbital xz at half-filling. Lower panel: Optimal BCS parameters for orbital yz at half-filling

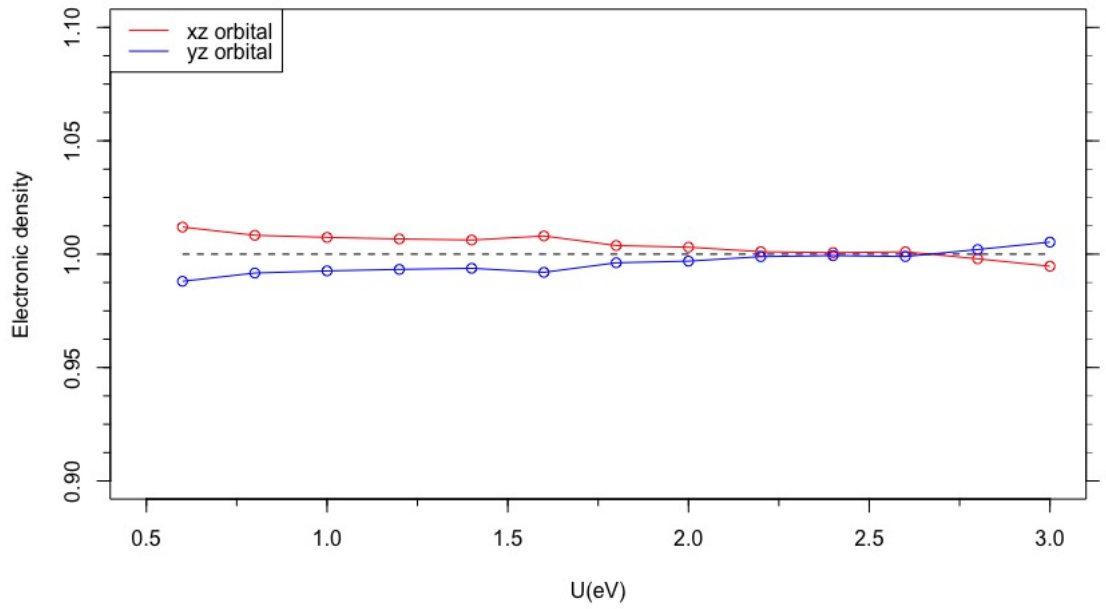

Figure 4.12: Electronic density per orbital, as a function of U, obtained in half-filling regime

4.3.2 10% doping regime

In this regime there is no apparent orbital selectivity both for electron- and hole-*doping*, as can be seen in figure 4.13. The situation, for the hole-*doping* regime, is quite different from the 6×6 case; indeed here there is no longer the symmetry breaking in the BCS parameters, as shown in figure 4.15.

The electron-*doping* regime is coherent with its homologous in the 6×6 case. Indeed, as can be seen in figure 4.14 BCS parameters fluctuate around $\Delta_{\alpha,\delta} = 0$ (α labels the orbital). It is worth mentioning that The results on the 12x12 lattice for BCS parameters and orbital occupations have been obtained with different initial conditions. We obtained a uniform state not only when we used the initial parameters of a uniform state, but also when we used as initial parameters those of a broken symmetry state (obtained from the 6×6 calculations of Sec.4.2.2).

Now we discuss the results regarding superconductivity since the lattice is large enough to compute superconductive correlations. We begin with the hole-*doping* regime. In section 4.2.2 we advanced the hypothesis that the xz orbital could present superconductive correlations, however from figure 4.16 we can see that superconductive correlations rapidly fall to order of $10^{-3}/10^{-4}$ with the increasing of steps between the pairs. The same goes for yz orbital (see figure 4.16). Results for the three-orbital model tell us that correlations are strongly suppressed when they are of the order of 10^{-3}(see Marino et al. (2024)), suggesting that the xz orbital is not superconductive at 10% hole-*doping*. In the electron-*doping* regime correlations fall rapidly to $10^{-3}/10^{-4}$, meaning that

there is no sign of superconductivity in both orbitals (see fig.4.17)

In the end, it seems true that away from half filling superconductivity cannot emerge without orbital selectivity, in accordance with the results of the three-orbital model (Marino et al. (2024)).

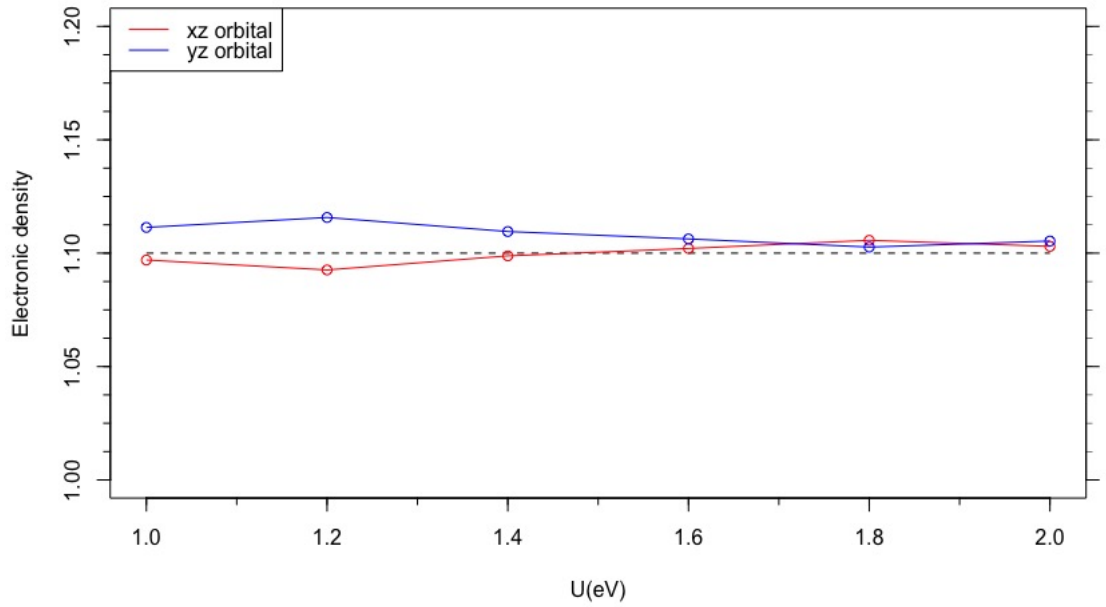

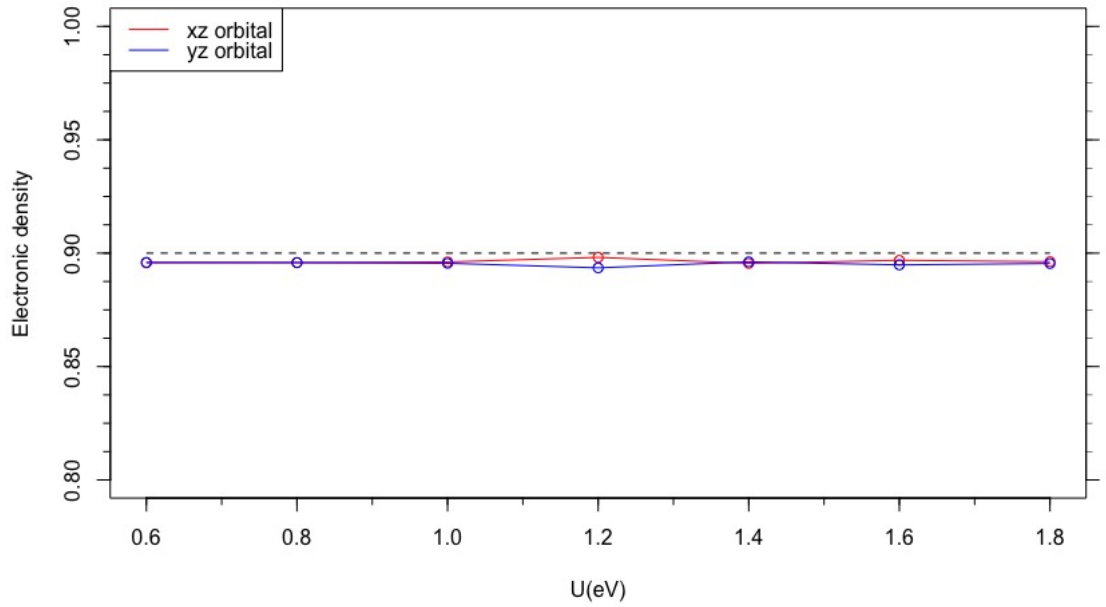

Figure 4.13: Upper panel: Electronic density of the two orbitals when the system is in 10% electron doping regime. Lower panel: Electronic density of the two orbitals when the system is in 10% hole doping regime.

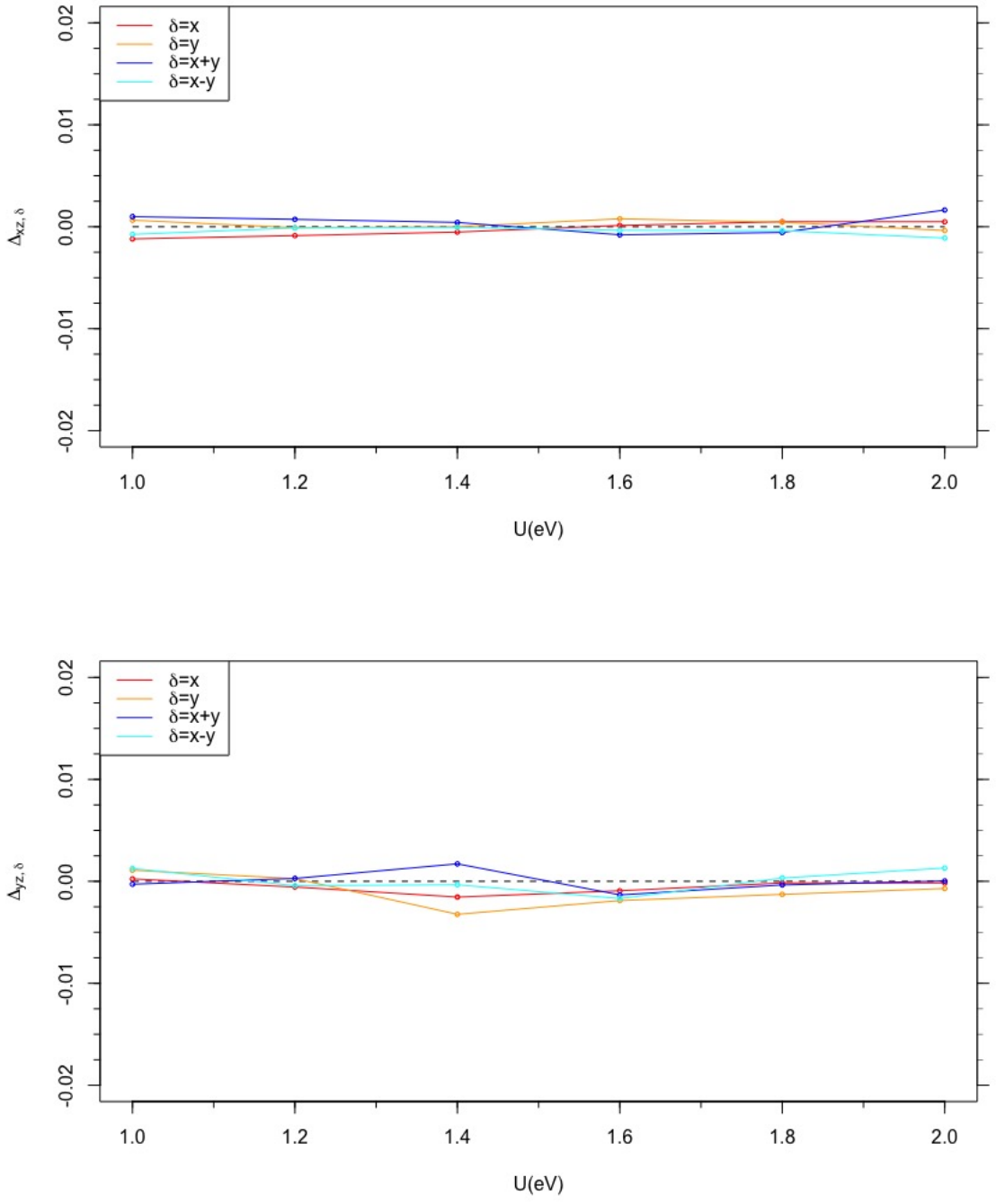

Figure 4.14: Upper panel: Optimal BCS parameters for orbital xz at 10% electron doping. Lower panel: Optimal BCS parameters for orbital yz at 10% electron doping

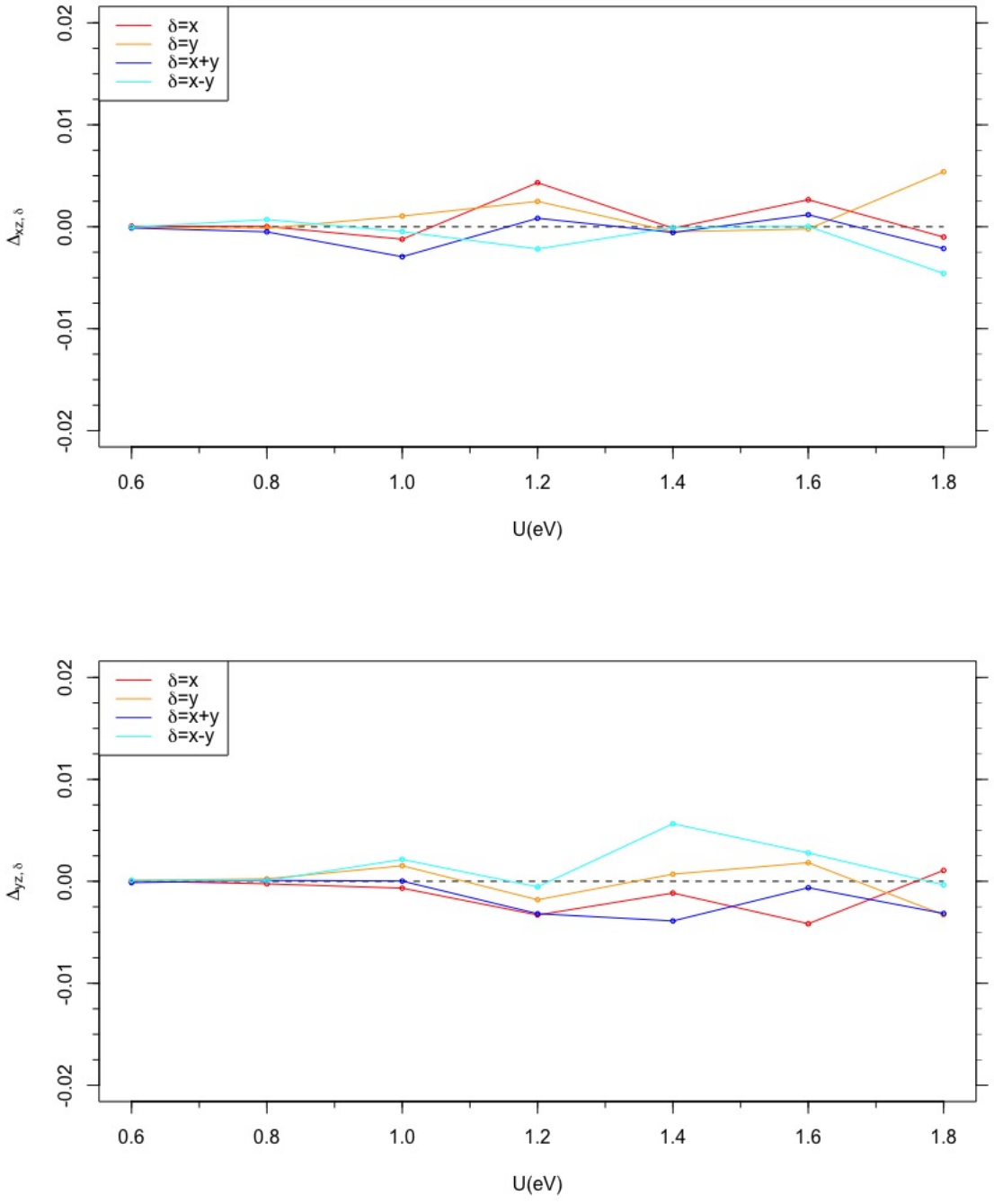

Figure 4.15: Upper panel: Optimal BCS parameters for orbital xz at 10% hole doping. Lower panel: Optimal BCS parameters for orbital yz at 10% hole doping

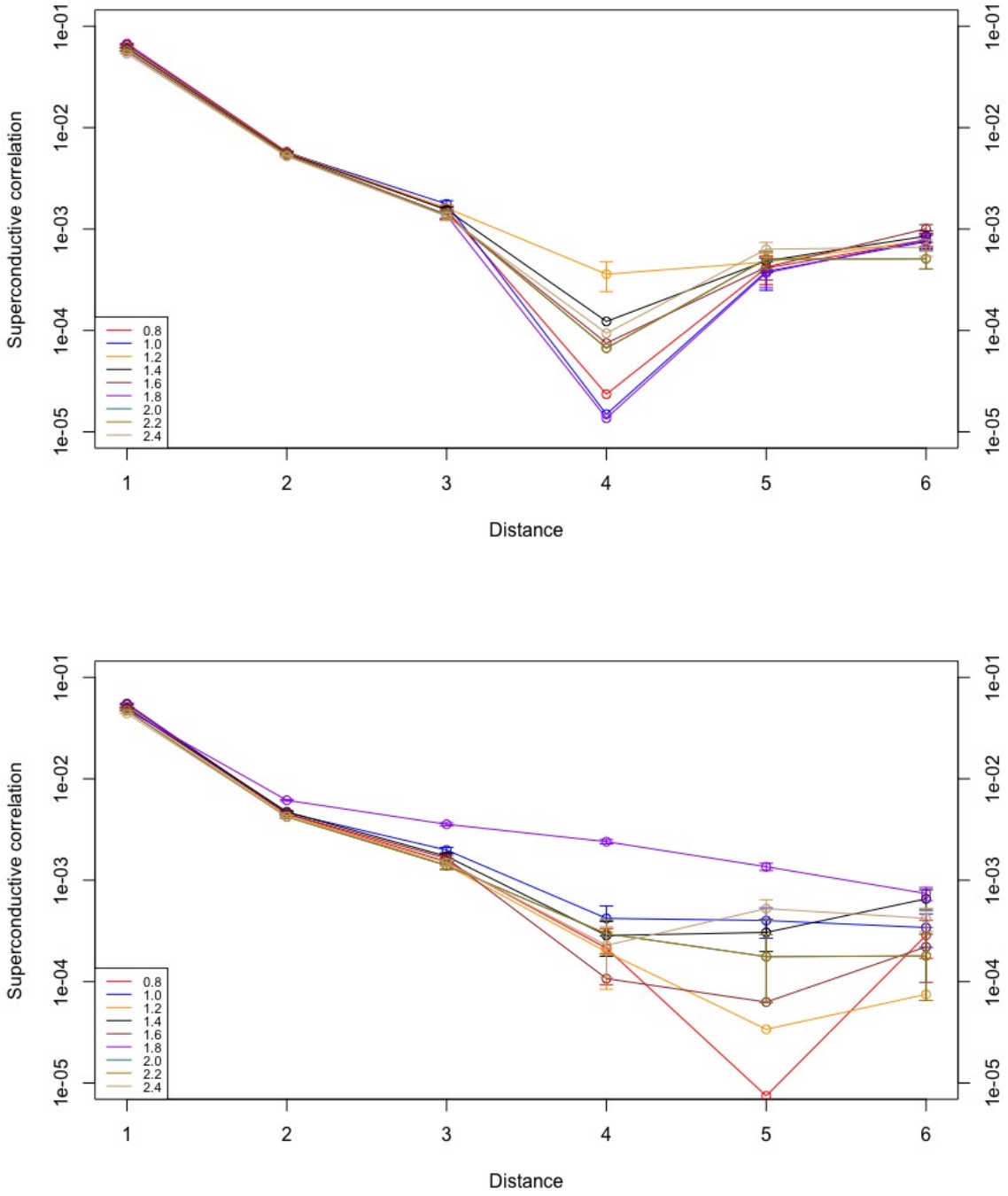

Figure 4.16: Upper panel: Pairing correlations for orbital xz at 10% hole doping. Lower panel: Pairing correlations for orbital yz at 10% hole doping. Values have been computed for $U \in (0.8, 2.4)$eV with a 0.2 step. Values are reported in logarithmic scale.

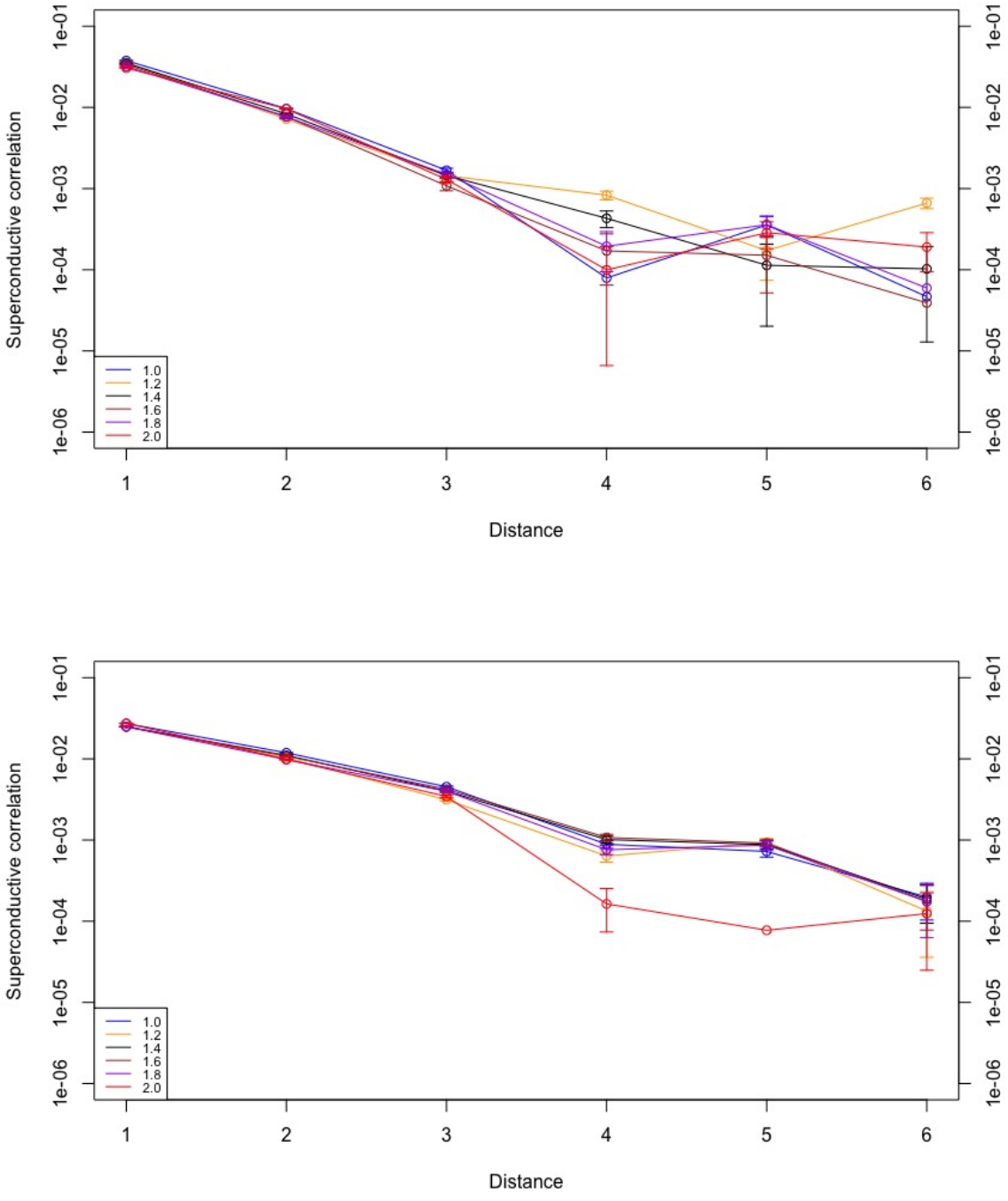

Figure 4.17: Upper panel: Pairing correlations for orbital xz at 10% electron doping. Lower panel: Pairing correlations for orbital yz at 10% electron doping. Values have been computed for $U \in (1.0, 2.0)$eV with a 0.2 step. Values are reported in logarithmic scale.

4.4 20% doping regime

We now move to the 20% *doping* regime. In this case results do not differ much from the 6×6 lattice (see section4.2.3). Again, no orbital is favored both in electron- and hole-*doping* regimes, as shown in figure 4.18. The BCS parameters do not show any significant deviation from zero for the two orbitals in both regimes (see figures 4.20 and 4.19), which had to be expected since there is no orbital selectivity. Again, these results have been obtained both from an initial state with broken symmetry and a uniform one.

From previous calculations in the 10% *doping* regimes, we can already expect superconductivity not to be present also in this case. Indeed, as shown in figure 4.21 and figure 4.22, superconductive correlations decay to the order of $10^{-3}/10^{-4}$ (some even 10^{-6}) already after the third step. Again we found out that superconductivity is not present contemporary with the fact that orbital selectivity is not present. It is worth mentioning that for the xz orbital some correlations fall to a value larger than 10^{-3}, however the BCS delta observed for that orbital (fig.4.20) are not significantly different from zero, hence we can safely assume the orbital not to be superconductive.

In the light of the results presented in this chapter, it is reasonable to assume that superconductivity cannot be present without orbital selectivity. Indeed, from calculations carried out in the three-orbital model, the emergence of superconductivity is linked with the presence of orbital selectivity (Marino et al. (2024)). This means that the two-orbital model is incapable of capturing the low-energy properties of IBS, probably due to the lack of a third orbital. Calculations showed that in the three-orbital model Hund's coupling causes two orbitals having an occupation near half-filling in different *doping* regimes, leading to orbital selectivity, i.e. the third orbital has a larger occupation, and superconductivity (Marino et al. (2024)). This is proved by the fact that if calculations are repeated with $J = 0$ superconductivity vanishes (Marino et al. (2024)).

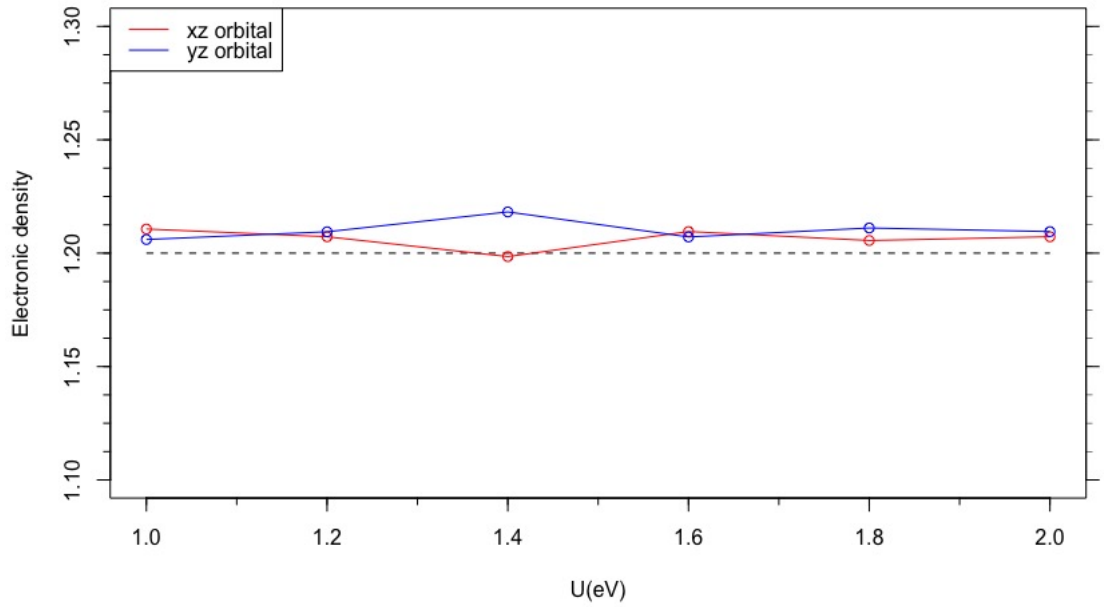

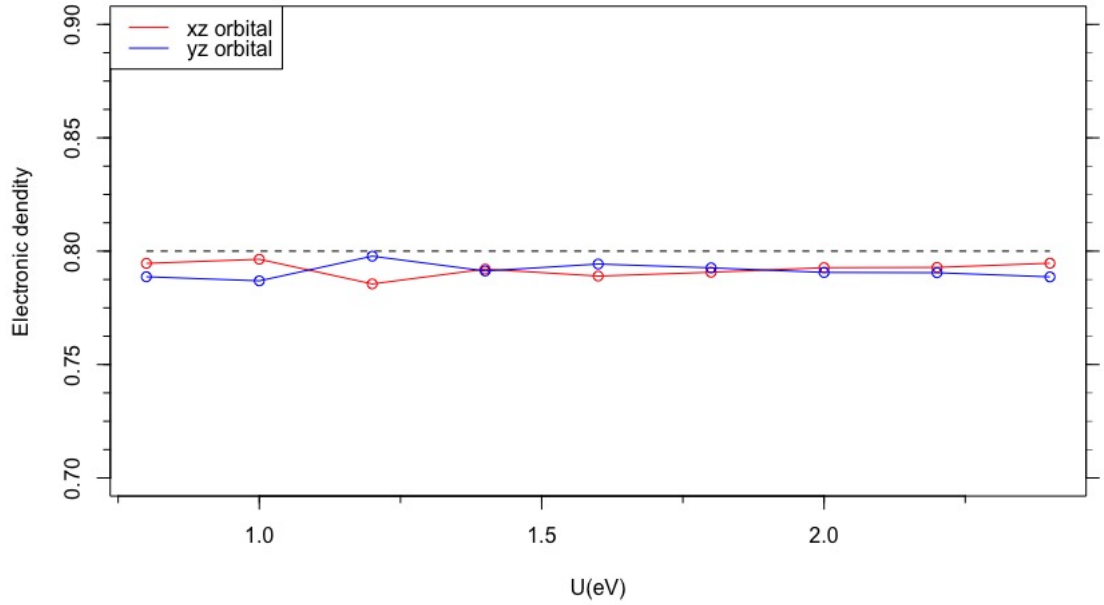

Figure 4.18: Upper panel: Electronic density of the two orbitals when the system is in 20% electron doping regime. Lower panel: Electronic density of the two orbitals when the system is in 20% hole doping regime.

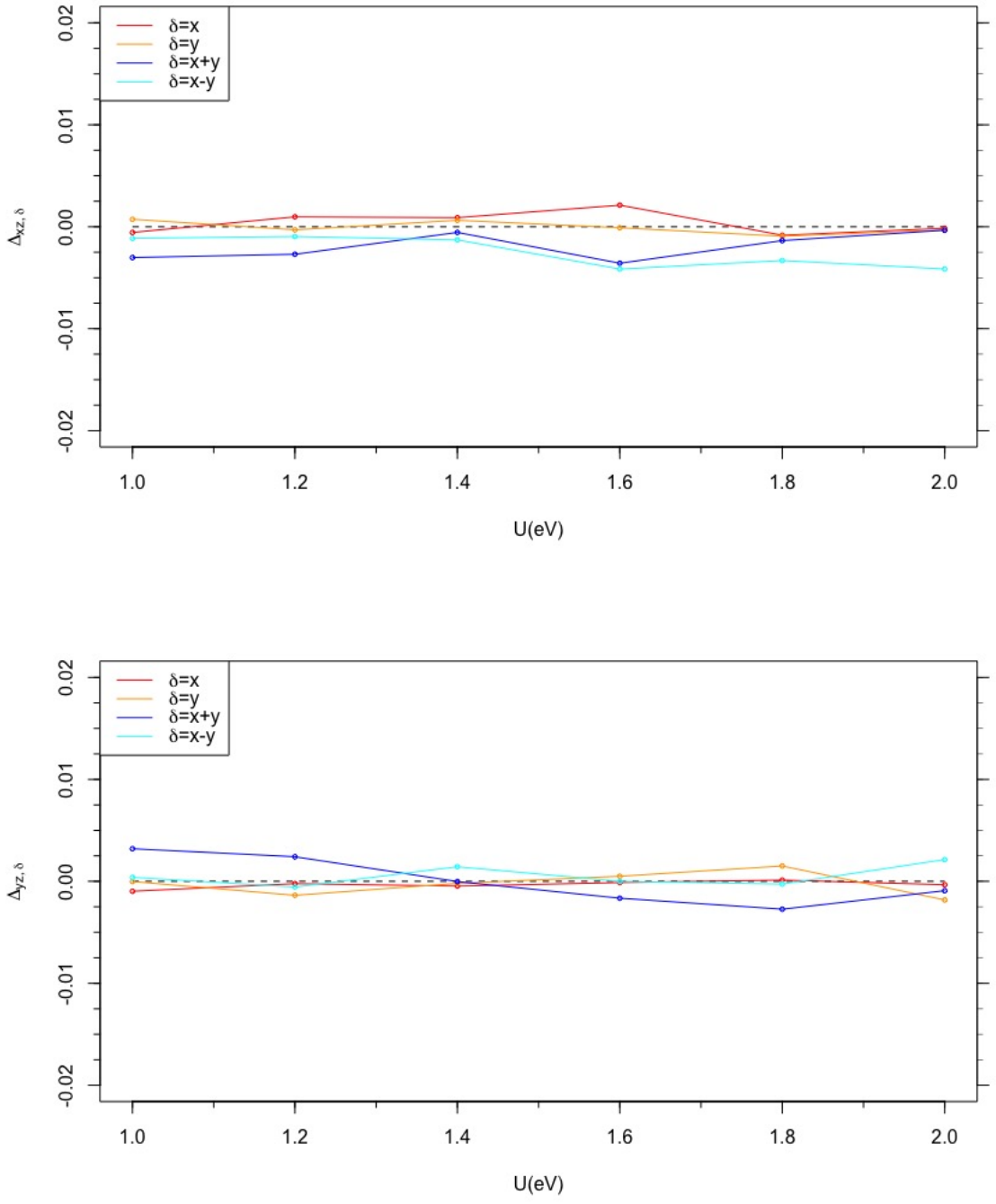

Figure 4.19: Upper panel: Optimal BCS parameters for orbital xz at 20% electron doping. Lower panel: Optimal BCS parameters for orbital yz at 20% electron doping

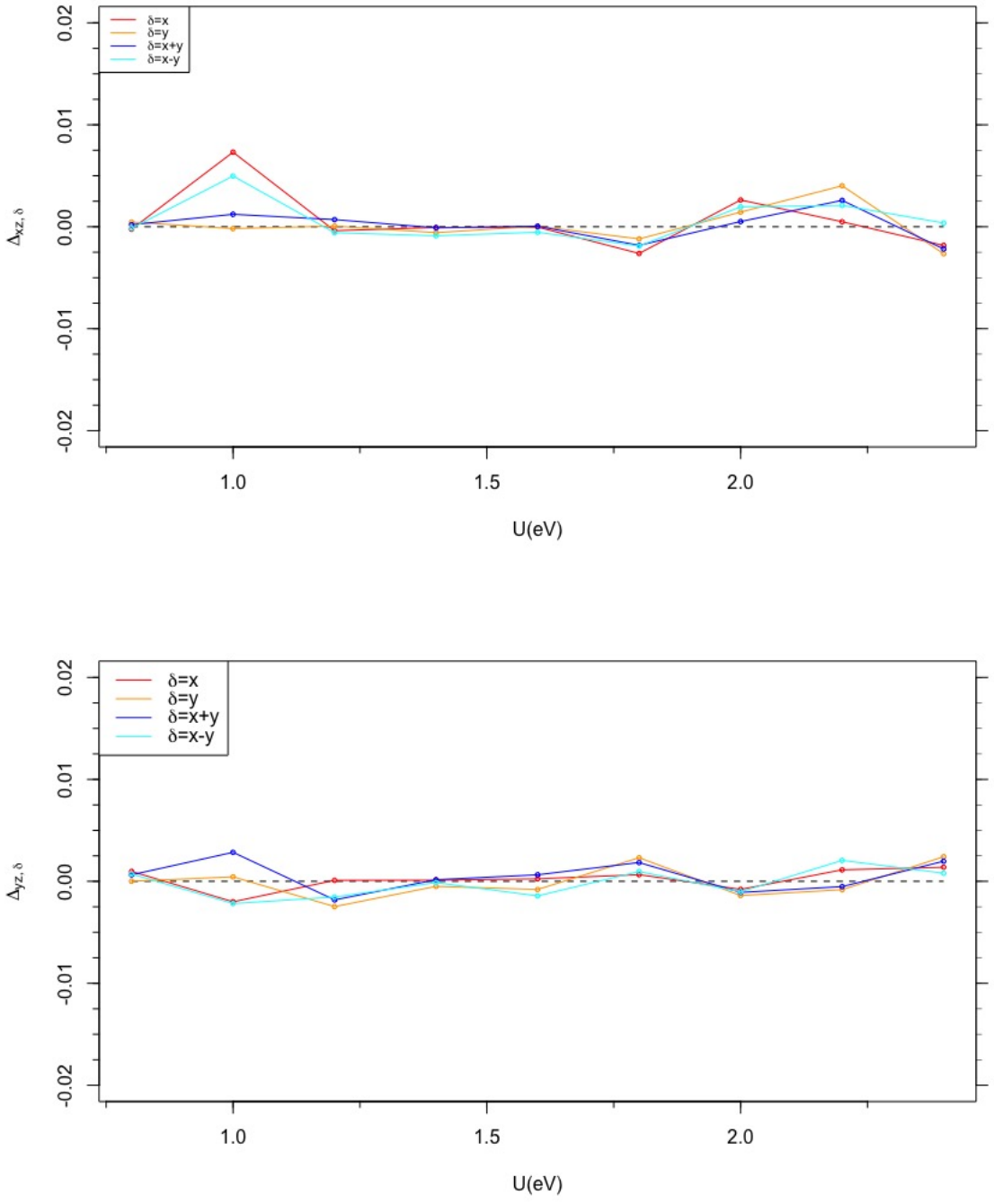

Figure 4.20: Upper panel: Optimal BCS parameters for orbital xz at 20% hole doping. Lower panel: Optimal BCS parameters for orbital yz at 20% hole doping

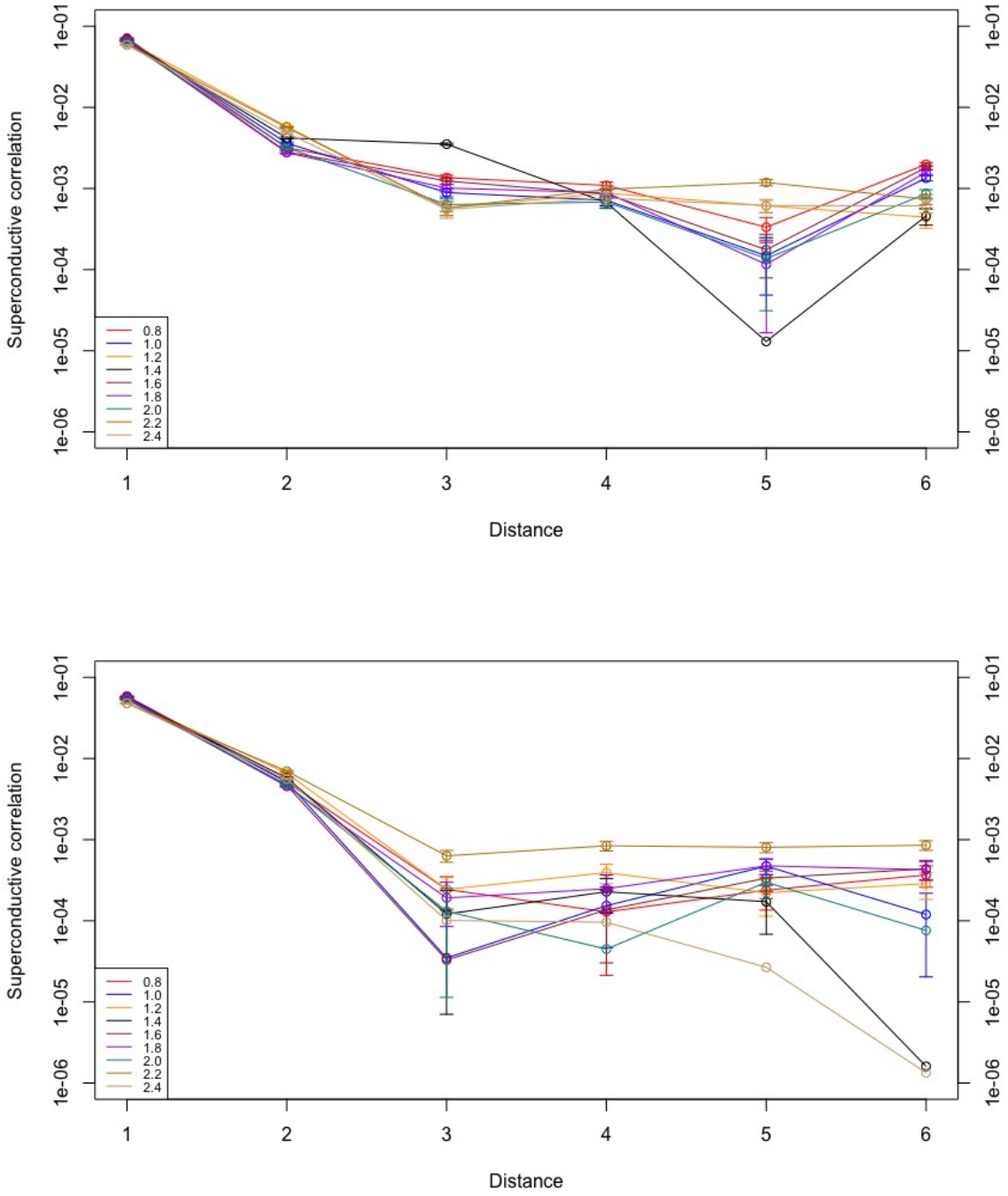

Figure 4.21: Upper panel: Pairing correlations for orbital xz at 20% hole doping. Lower panel: Pairing correlations for orbital yz at 20% hole doping. Values have been computed for $U \in (0.8, 2.4)$eV with a 0.2 step. Values are reported in logarithmic scale.

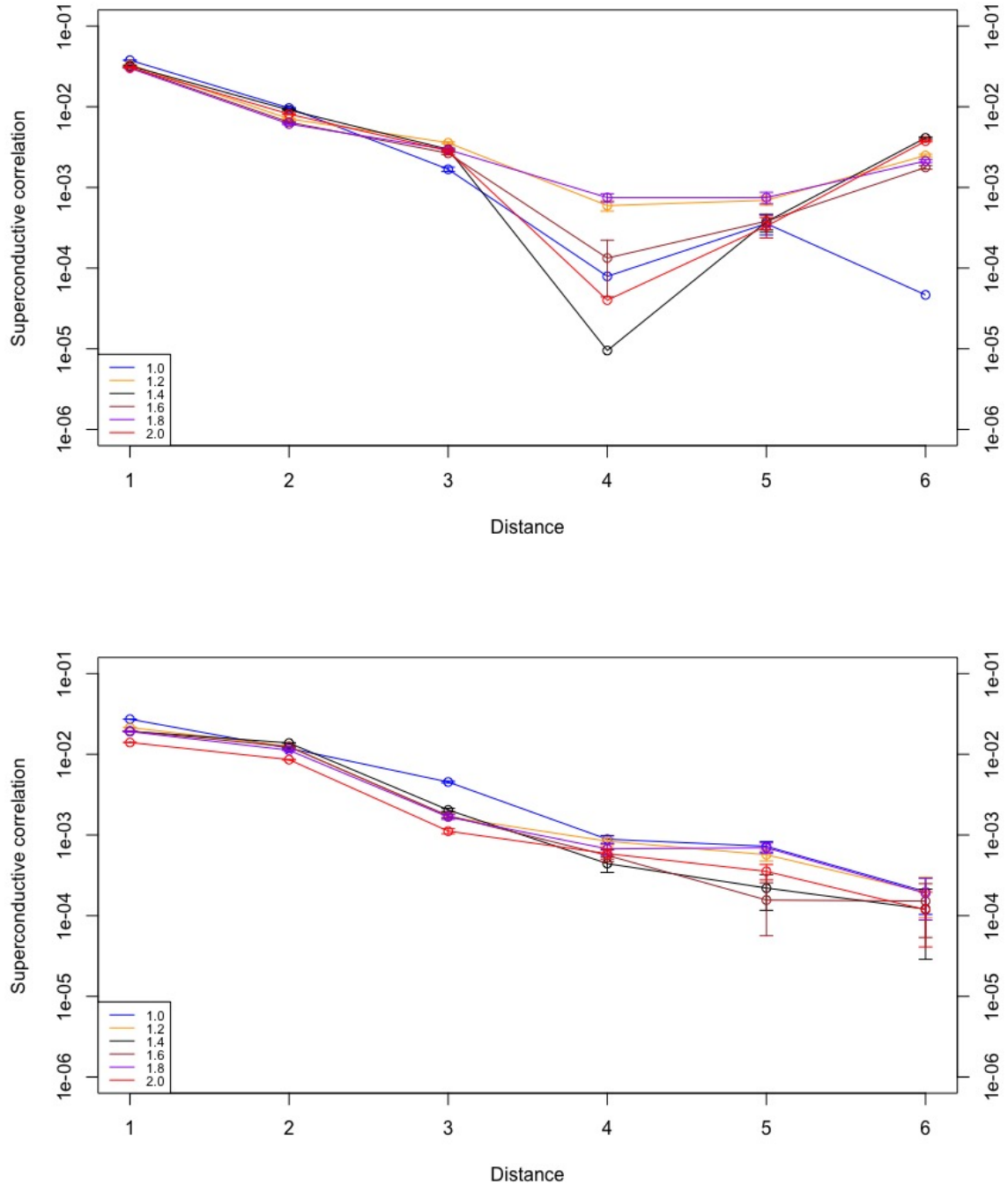

Figure 4.22: Upper panel: Pairing correlations for orbital xz at 20% electron doping. Lower panel: Pairing correlations for orbital yz at 20% electron doping. Values have been computed for $U \in (1.0, 2.0)$eV with a 0.2 step. Values are reported in logarithmic scale.

Chapter 5

Conclusion

In this thesis we have considered the two-orbital Hubbard model with Kanamori interactions in order to understand if it could capture low-energy properties, especially superconductivity, in iron-based superconductors. Low-energy properties have been investigated with the use of variational wavefunctions and Variational Monte Carlo techniques.

We first investigated the Fermi surface without correlations and found out that it consists of two electron-like pockets and two hole-like pockets, in agreement with what has been found by other calculations (Raghu et al. (2010)).

We then included correlations using Jastrow factors to analyze superconductive correlations. In order to understand the behavior of the variational wavefunction, we first studied the model on a 6×6 lattice, with two orbitals per site, in different doping regimes: half-filling, 10% hole/electron-*doping* and 20% hole/electron-*doping*. We were interested in finding out if the system could present orbital selectivity features in regimes far from half-filling, inspired by the results on the link between superconductivity and orbital selectivity in the three-orbital Hubbard model (Marino et al. (2024)), and found out that, in 10% hole-*doping* regime, orbital selectivity actually appears together with the fact that BCS parameters are different from zero for large values of Hubbard U, a necessary condition for superconductivity to appear. In order to compute superconductive correlations we needed to move to a larger lattice, hence we considered a 12×12 lattice. We investigated again the different regimes mentioned above using as initial state both one with a broken symmetry between the two orbitals and a uniform one. We obtained, in all regimes, uniform solutions for the orbital occupations, i.e. no orbital selectivity, and in most cases BCS variational parameters were oscillating around zero. We then moved to investigate the superconductive correlations studying the correlation between two pairs of electrons, made by electrons along y, while one was moving along x and the other remained fixed in place. Results showed that in almost all cases the correlations rapidly fell to the order of $10^{-3}/10^{-4}$, and by confronting them with the results obtained for the three-orbital model (Marino et al. (2024)), where correlations of those orders of magnitude are considered strongly suppressed, we can say that also in the two-orbital model such correlations are

strongly suppressed, i.e. the two orbitals do not become superconductive.

Based on these results and those of the three-orbital model (Marino et al. (2024)) we can say that there is a link between superconductivity and orbital selectivity. Indeed, there is no superconductivity without orbital selectivity.

The absence of orbital selectivity, hence of superconductivity, suggests that the two-orbital model is inadequate for describing iron-based superconductors. This implies that the d_{xy} orbital is actually fundamental to describe IBS. The d_{xy} was excluded due to the fact that it is irrelevant in the definition of the Fermi surface at $U = 0$ (Raghu et al. (2010), Marino et al. (2024)); however it turned to be crucial when investigating superconductivity.

Bibliography

Becca, F. and Sorella, S. (2017). *Quantum Monte Carlo approaches for correlated systems*. Cambridge University Press.

Bordoloi, A., Zannier, V., Sorba, L., Schönenberger, C., and Baumgartner, A. (2022). Spin cross-correlation experiments in an electron entangler. *Nature*, 612(7940):454–458.

Capello, M., Becca, F., Fabrizio, M., Sorella, S., and Tosatti, E. (2005). Variational description of mott insulators. *Phys. Rev. Lett.*, 94:026406.

Capone, M. (2018). Orbital-selective metals. *Nature materials*, 17(10):855–856.

Cooper, L. N. (1956). Bound electron pairs in a degenerate fermi gas. *Physical Review*, 104(4):1189.

Daghofer, M., Nicholson, A., Moreo, A., and Dagotto, E. (2010). Three orbital model for the iron-based superconductors. *Physical Review B—Condensed Matter and Materials Physics*, 81(1):014511.

de' Medici, L., Giovannetti, G., and Capone, M. (2014). Selective mott physics as a key to iron superconductors. *Phys. Rev. Lett.*, 112:177001.

De'Medici, L. and Capone, M. (2017). Modeling many-body physics with slave-spin mean-field: Mott and hund's physics in fe-superconductors. *The Iron Pnictide Superconductors: An Introduction and Overview*, pages 115–185.

Fernandes, R. M. and Chubukov, A. V. (2016). Low-energy microscopic models for iron-based superconductors: a review. *Reports on Progress in Physics*, 80(1):014503.

Georges, A., Medici, L. d., and Mravlje, J. (2013). Strong correlations from hund's coupling. *Annu. Rev. Condens. Matter Phys.*, 4(1):137–178.

Giuliani, G. and Vignale, G. (2005). *Quantum Theory of the Electron Liquid*. Cambridge University Press.

Hastings, W. K. (1970). Monte carlo sampling methods using markov chains and their applications.

Marino, V., Scazzola, A., Becca, F., Capone, M., and Tocchio, L. F. (2024). Intertwined superconductivity and orbital selectivity in a three-orbital hubbard model for the iron pnictides. *arXiv preprint arXiv:2406.13634*.

Metropolis, N., Rosenbluth, A. W., Rosenbluth, M. N., Teller, A. H., and Teller, E. (1953). Equation of state calculations by fast computing machines. *The journal of chemical physics*, 21(6):1087–1092.

Mott, N. F. (1949). The basis of the electron theory of metals, with special reference to the transition metals. *Proceedings of the Physical Society. Section A*, 62(7):416.

Raghu, S., Qi, X.-L., Liu, C.-X., Scalapino, D., and Zhang, S.-C. (2010). A minimal two-band model for the superconducting fe-pnictides. *Phys. Rev. B*, 77:220503.

Sorella, S. (1998). Green function monte carlo with stochastic reconfiguration. *Phys. Rev. Lett.*, 80:4558–4561.

Sorella, S. (2001). Generalized lanczos algorithm for variational quantum monte carlo. *Phys. Rev. B*, 64:024512.